THE UNIVERSITY OF ALBERTA

A SOLID-STATE CHARGE-SENSITIVE AMPLIFIER FOR THE DETECTION OF HIGH VELOCITY MICRO-PARTICLES

by

BRUCE THOMAS DIPPIE

A THESIS

SUBMITTED TO THE FACULTY OF GRADUATE STUDIES

IN PARTIAL FULFILLMENT OF THE REQUIREMENTS FOR THE DEGREE

OF MASTER OF SCIENCE

DEPARTMENT OF ELECTRICAL ENGINEERING

EDMONTON, ALBERTA

JULY 1966

UNIVERSITY OF ALBERTA

FACULTY OF GRADUATE STUDIES

The undersigned certify that they have read, and recommend to the Faculty of Graduate Studies for acceptance, a thesis entitled A Solid-State Charge-Sensitive Amplifier for the Detection of High Velocity Micro-Particles submitted by Bruce Thomas Dippie in partial fulfillment of the requirements for the degree of Master of Science.

ABSTRACT

The major portion of this thesis describes the design of a wideband solid-state charge-sensitive amplifier which has an insulated-gate field-effect transistor for the input device. The amplifier is suitable for the detection of high velocity micro-particles.

A generalized charge-sensitive amplifier is first examined and design criteria are obtained.

Special attention is given to the noise properties of charge-sensitive amplifiers and metal-oxide-semiconductor field-effect transistors. Equations for the noise performance of charge-sensitive amplifiers are derived.

The operation of a micro-particle charger is briefly described, and the performance of the charger is examined by using the charge-sensitive amplifier to detect the particles.

When lower noise insulated-gate field-effect transistors are available the amplifier will be suitable for nuclear work.

ACKNOWLEDGEMENTS

The research described in this thesis was carried out at the Department of Electrical Engineering, University of Alberta, under the supervision of E.M.Edwards, to whom the author is indebted for his advice and guidance.

The author would also like to thank the staff members and graduate students, in particular W.J.Haydamack and F.E. Vermeulen, of the Department for their suggestions and assistance. As well, the author would like to express his appreciation for the continued encouragement given by his wife Marge during the preparation of this work.

The author is further indebted to the National Research Council and the University of Alberta for financial assistance.

TABLE OF CONTENTS

LIST OF FIGURES

I INTRODUCTION

Meteoroids, particles traveling in outer space, present a potential hazard to space travel. The high rate of bombardment of space vehicles by minute micrometeoroids is of prime concern to space scientists.

1.1 Micrometeoroids

Micrometeoroids range in size from about 0.3 to 300 microns in diameter(1) and travel at velocities of 11 to 73 km/sec.(2) Their composition is chiefly combinations of iron, nickel, and stone.(3) Their flux rates can be as high as 1.4 impacts/m^2-sec for small micrometeoroids.(4) Consequently, there are continual collisions between space vehicles and micrometeoroids. These collisions could damage pressurized cabins, space suits, propellant tanks, optical lenses, heat shields, and other exposed materials.

Although much information has been gained from the space craft, satellites, and space probes that have contained meteoroid detectors, the need for improved detectors and the need to study the effects of hypervelocity impacts on engineering materials make it necessary to simulate micrometeoroids in the laboratory. This can be done by accelerating suitable particles to appropriate velocities.

1.2 Production of Artificial Micrometeoroids

At the University of Alberta micro-particles of the desired size, shape, density, and composition are charged and accelerated by an electric field This is done in a high vacuum to prevent breakdown and to avoid friction losses.

The charging mechanism, shown in Figure 1.1, contains a tray loaded with carbonyl iron spheres of twenty micron average diameter. The electric field in the first chamber agitates the particles in the tray. This causes some particles to enter the second chamber, collide with the charged sphere, gain charge themselves, be repelled, and then be emitted through the aperture into a drift section.

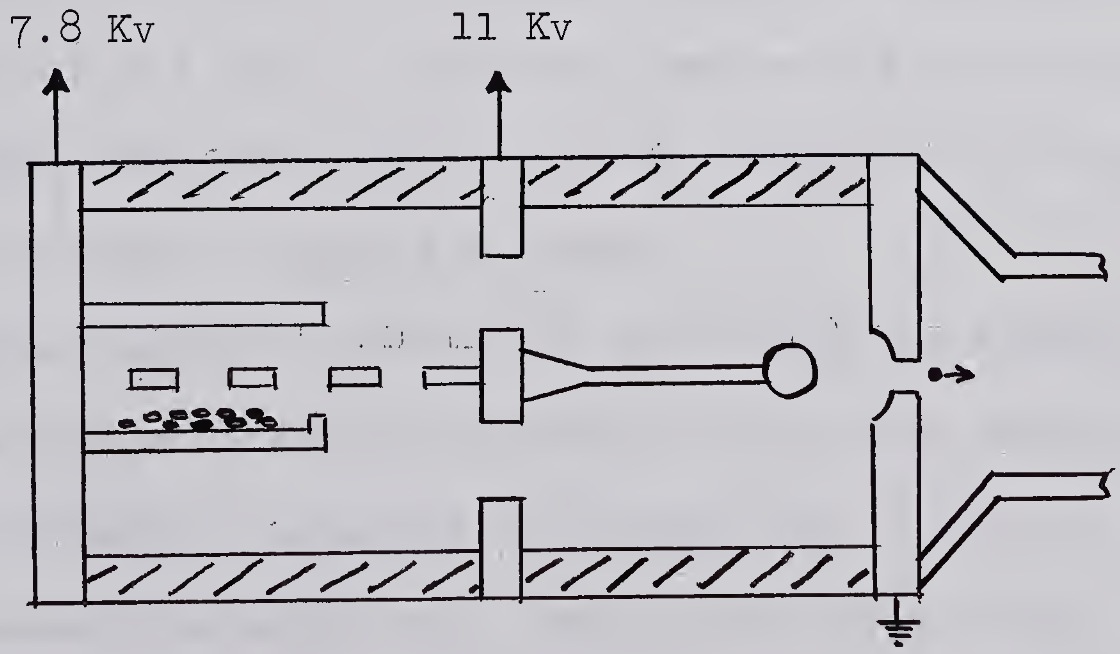

FIGURE 1.1 THE CHARGING MECHANISM

Further acceleration of these particles will require an accelerator capable of accepting the wide spread in charge-to-mass ratios of the emitted particles. A linear accelerator is suitable, but requires a detection system to give the data necessary to properly "phase" the accelerator.

1.3 Detection Methods

When a particle bombards a target the velocity must be known in order to relate the energy of impact to the damage which results.

One method of determining the velocity is to use a photomultiplier or a photodiode to detect light scattered from the particle as it passes intense light sources that are separated by known distances. The main advantages of this method are that it in no way impedes the progress of the particle and that it does not require the particle to be charged. Thus the charge could be stripped off of the particle before it impacts a target.

Another method of detection is to pass the charged particle through screened cylinders. The charge induced on these cylinders is detected by an amplifier - usually a "charge-sensitive amplifier". This method also allows the measurement of the charge on the particle. From a knowledge of its charge and velocity the mass and size of the particle can be determined.

To determine the mass and size of a charged particle the kinetic and electrical energies are equated:

$$QV = \frac{1}{2}mv^2$$

Therefore: $$m = \frac{2QV}{v^2} \qquad (1.1)$$

where: m is the mass in kilograms

Q is the particle charge in coulombs

v is the velocity in meters/second

and V is the accelerating voltage in volts

Since the particle density is known, and if the particle is assumed to be spherical, then:

$$r = \left\{\frac{3}{2}\,\frac{QV}{\pi\rho v^2}\right\}^{1/3} \qquad (1.2)$$

where: ρ is the density in kg/m^3

and r is the radius in meters

At present the detection system shown in Figure 1.2 is being used. The first detector triggers an oscilloscope; the second and third give the particle velocity; while the last, a collector, gives an accurate indication of the charge on the particle.

The collector, of course, would not be used if further acceleration is desired; but the detection system shown allows determination of the "effectiveness" of the charger.

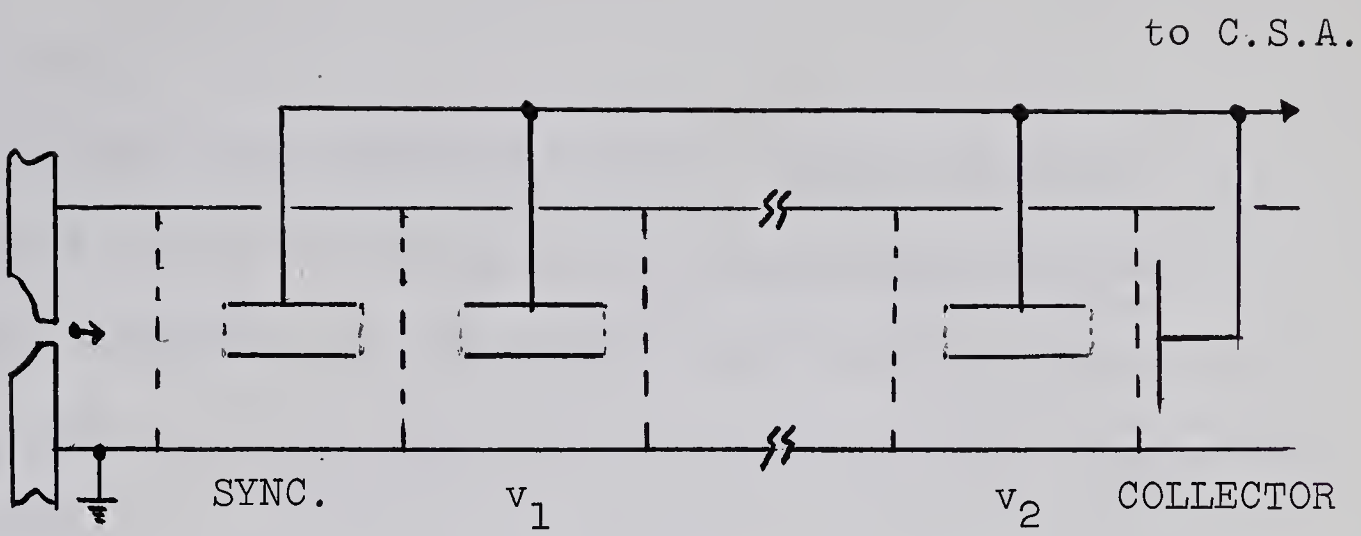

FIGURE 1.2 PARTICLE DETECTION SYSTEM

For a particle of radius r in contact with the charging sphere, of radius R, at a potential V the charge imparted to the particle is (for R > r):(5)

$$Q_r = \frac{2\pi^3 R r^2 \epsilon_0 V}{3(R+r)^2} \quad \text{coulombs} \tag{1.3}$$

where: $\epsilon_0 = 8.85 \times 10^{-12}$ farads/meter

Hence the expected charge-to-mass ratio can be compared to the measured charge-to-mass ratio.

This thesis is concerned with the properties, design, construction, and performance of a solid-state charge-sensitive amplifier suitable for the detection of high velocity micro-particles produced in the laboratory.

II CHARGE-SENSITIVE AMPLIFIER

2.1 Source

The particle detection system, shown in Figure 1.2, acts as a source of charge with a capacitance C_D. The leakage resistance of the source can be neglected as it is much larger than the capacitive reactance at all frequencies of concern.

The signal appearing at the input of the amplifier is the charge induced on the cylinders and, ideally, is a step of charge. The screen-to-detector transition regions cause the input signal to have a finite rise time; but, amplifier performance can be predicted using a step input.

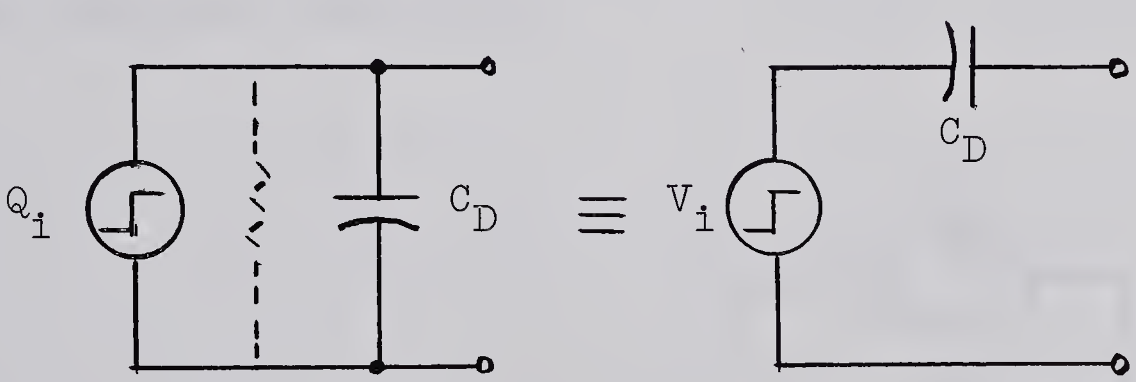

FIGURE 2.1 REPRESENTATION OF THE SOURCE

The charge source can be transformed into a voltage source (Figure 2.1) by using Thevenin's Theorem. The voltage source is more readily suited to the normal voltage transfer

function analysis. If the input charge function is causal, then in the frequency domain:

$$V_i(s) = \frac{Q_i(s)}{C_D} \tag{2.1}$$

where: s is the complex frequency.

2.2 Transfer Function of a Charge-Sensitive Amplifier

A charge-sensitive amplifier is shown in Figure 2.2. Finite input impedance is represented by R_A in parallel with C_A, and finite negative open loop gain is denoted by -A. The amplifier is assumed to have no upper corner frequency and zero output impedance. The feedback capacitor C_F makes the amplifier charge sensitive, while R_F stabilizes the amplifier under quiescent conditions.

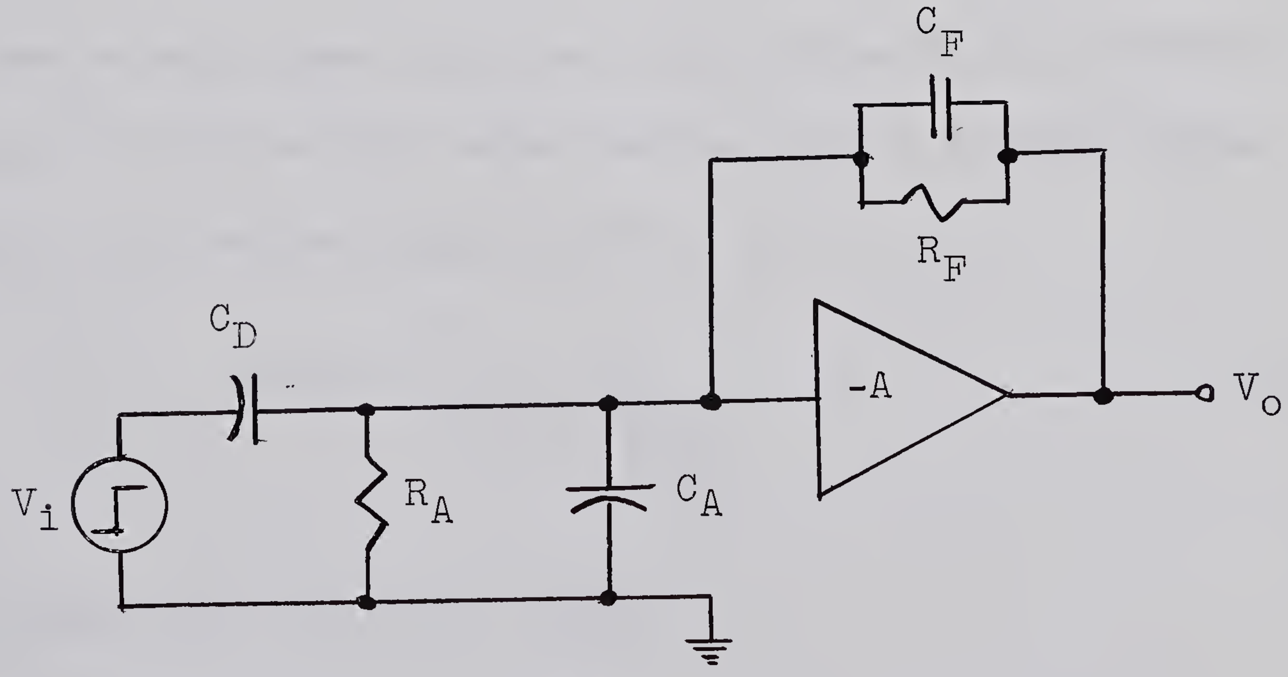

FIGURE 2.2 CHARGE-SENSITIVE AMPLIFIER

The expression for the closed loop transfer function of a general feedback amplifier is given by:(6)

$$H = \frac{V_o}{V_i} = -\frac{Z_F}{Z_I}\,\frac{1}{1+\frac{1}{A}\left(1+\frac{Z_F}{Z_I//Z_A}\right)} \qquad (2.2)$$

For the charge-sensitive amplifier:

$$Z_A = \frac{R_A}{1+sR_AC_A}, \qquad Z_F = \frac{R_F}{1+sR_FC_F}, \qquad Z_I = \frac{1}{sC_D}$$

Then:

$$\begin{aligned} H(s) &= \frac{V_o(s)}{V_i(s)} \\ &= -\frac{C_D}{C_F}\,\frac{AC_F}{C_D+C_A+C_F(1+A)}\,\frac{s}{s+\dfrac{1}{\dfrac{R_FR_A}{R_F+R_A(1+A)}\left(C_D+C_A+C_F(1+A)\right)}} \end{aligned} \qquad (2.3)$$

For a large open loop gain, and since R_A is generally greater than R_F and all capacitances are of similar value, Equation 2.3 reduces approximately to:

$$H(s) = -\frac{C_D}{C_F}\,\frac{s}{s+\frac{1}{R_FC_F}} \qquad (2.4)$$

Or, in terms of the input charge:

$$V_o(s) = -\frac{Q_i(s)}{C_F}\,\frac{s}{s+\frac{1}{R_FC_F}} \qquad (2.5)$$

It is seen from Equations 2.4 and 2.5 that the output voltage is approximately independent of all amplifier parameters and depends only on the external and known R_F and C_F. Further, Heywood(7) has shown that the sensitivity of the amplifier to changes in both open loop gain and detector capacitance is reduced by the loop gain factor. Heywood has also drawn a comparison to a voltage-sensitive amplifier (for which the feedback is resistive) and has shown that the voltage-sensitive amplifier is more sensitive to changes in the detector capacitance. And, for the voltage-sensitive amplifier, both the detector and amplifier capacitances need to be known in order to determine the applied input charge. As well, Heywood has stated that the two types of amplifiers are similar in performance from a noise point of view because the noise contributions of the feedback networks cause only a small degradation of the total signal-to-noise ratio. For a charge-sensitive amplifier, with thermal or 1/f noise dominating, this is the case if C_F is small compared to $C_A + C_D$. This is shown in Chapter 4. For these reasons the charge-sensitive amplifier is better suited to the detection of micro-particles.

2.3 High Frequency Effects

In any practical amplifier parasitic capacitances cause the gain to fall off at high frequencies. By cascading the ideal amplifier with a low pass filter of transfer function F(s), a new transfer function representing the actual amplifier is formed.

It is assumed that the closed loop high frequency roll-off starts at ω_H and is initially -20 db/decade changing to -40 db/decade at $a\omega_H$ $(a > 1)$.

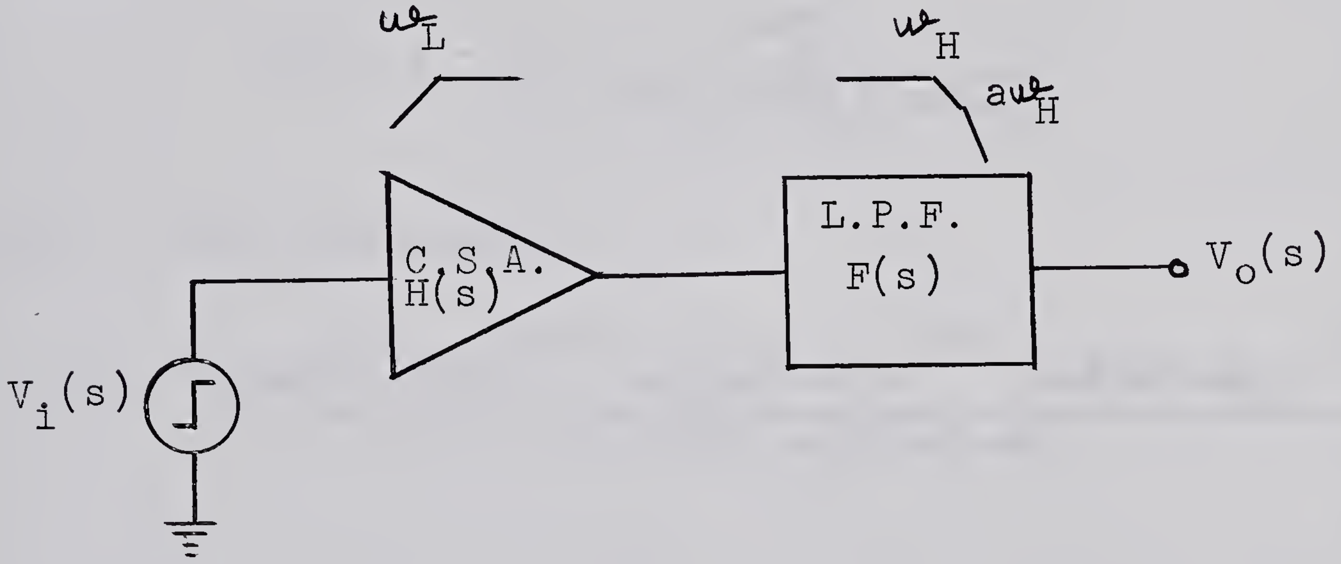

FIGURE 2.3 REPRESENTATION OF A PRACTICAL AMPLIFIER

Thus:

$$F(s) = \frac{a\omega_H^2}{(s+\omega_H)(s+a\omega_H)} \qquad (2.6)$$

The new transfer function is:

$$G(s) = H(s)F(s)$$

$$G(s) \simeq A_c \frac{a\omega_H^2 s}{(s+\omega_L)(s+\omega_H)(s+a\omega_H)} \qquad (2.7)$$

where: $A_c = -\dfrac{C_D}{C_F}$

and $\omega_L = \dfrac{1}{R_F C_F}$

2.4 Response to a Step of Charge

For a step of charge of height Q_i,

$$Q(s) = \frac{Q_i}{s}$$

Then:

$$V_o(s) = -\frac{Q_i}{C_F} \frac{a\omega_H^2}{(s+\omega_L)(s+\omega_H)(s+a\omega_H)} \qquad (2.8)$$

Or, in the time domain:

$$v_o(t) = -\frac{Q_i}{C_F} \frac{a\omega_H^2 (a-1) e^{-\omega_L t} - a\omega_H (a\omega_H - \omega_L) e^{-\omega_H t} + a\omega_H (\omega_H - \omega_L) e^{-a\omega_H t}}{(a-1)(\omega_H - \omega_L)(a\omega_H - \omega_L)} \qquad (2.9)$$

For a wideband amplifier $\omega_H \gg \omega_L$ and so:

$$v_o(t) \simeq -\frac{Q_i}{C_F} \left[e^{-\omega_L t} - \frac{e^{-\omega_H t}}{(a-1)} \left(a - e^{-(a-1)\omega_H t}\right) \right] \qquad (2.10)$$

An indication of the speed with which the amplifier responds to a step is given by the rise time, t_R in Figure 2.4.

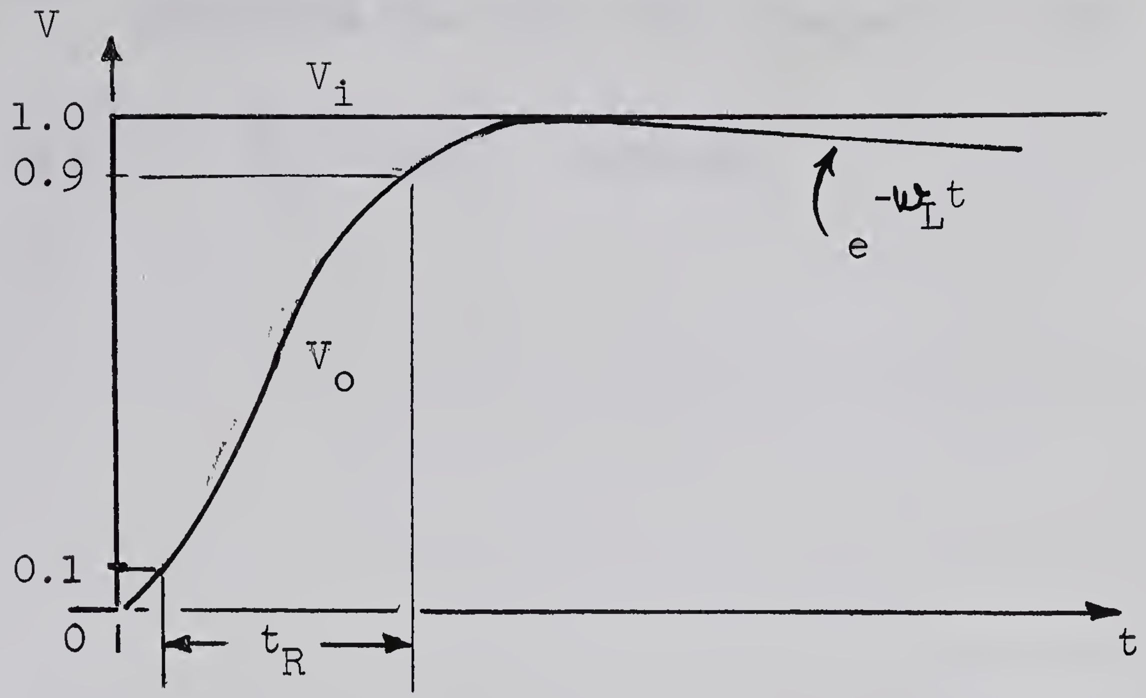

FIGURE 2.4 AMPLIFIER STEP RESPONSE

If $\omega_L \ll \omega_H$ and if $a > 5$ then the rise time can be approximated by:

$$t_R = \frac{2.2}{\omega_H} \quad \text{seconds} \tag{2.11}$$

The actual input is not a step of charge and the above analysis can be modified to account for the finite rise time of the input signal. It follows that the output signal will be an accurate representation of the input if the rise time of the amplifier is much less than the rise time of the input signal.

To obtain an accurate measurement of the input charge and to obtain a good reproduction of the input, the output should decay very little during the time that the input

charge is applied. If $\omega_L \ll \omega_H$, the decay is determined by $e^{-\omega_L t}$. Therefore the hold time constant is $1/\omega_L$.

$$\text{Or:} \qquad \tau_L = R_F C_F \quad \text{seconds.} \tag{2.12}$$

III AMPLIFIER REQUIREMENTS

The micro-particle charger and the particle detection system set the criteria of the charge-sensitive amplifier.

3.1 Input Device Selection

The input device should have low noise and high input impedance. A very high input resistance enables a long hold time constant to be obtained with a small feedback capacitor. Then C_F can be smaller than the detector capacitance and the system will have gain. Low noise is required to detect those particles that have little charge on them - the minimum charge expected is 10^{-14} coulombs.

Two semiconductor devices that have inherently high input impedances are available: the junction Field-Effect Transistor (FET) and the relatively new Metal-Oxide-Semiconductor Field-Effect Transistor (MOSFET) - also known as the Insulated-Gate FET or the Surface FET.

The use of FETs in charge-sensitive amplifiers has been investigated previously.(8,9,10) The MOSFET has an extremely high input resistance (10^{13} to 10^{17} ohms) and hence a very low input leakage current, and is far superior to the junction FET in these respects. Also, the MOSFET is an inherently higher frequency device.(11) On the other hand, the transconductance (y_{fs}) of MOSFETs is generally lower and

1/f noise is much more predominant than for junction FETs. Because the advantages of the MOSFET make it a better device for fast wideband charge-sensitive amplifiers and because the disadvantages of the MOSFET are largely technological and are likely to be improved upon, it was decided to build a charge-sensitive amplifier using a MOSFET for the input device. The equivalent circuit, device terminology, and a brief theory of the operation of a MOSFET are given in Appendix I. MOSFET noise properties are discussed in Chapter 4 and some experimental results of the determination of the 1/f noise corner frequency are given in Appendix III.

3.2 Rise Time

The fastest particle, at present, has a velocity in the order of 0.5 km/sec. The smallest screen-to-detector transition region, at the collector plate, is about two millimeters long; therefore the particle traverses this distance in about four microseconds and all of its charge appears at the amplifier input in this time. Since rise times add approximately as the square root of the sum of the squares,(12) the output rise time will be increased only 1% if the amplifier has a rise time of 0.4 μsec. From Equation 2.11 the upper corner frequency should be greater than 875 KHz.

3.3 Hold Time

The slowest particle (50m/sec) takes 400μsec to pass through the cylinder length (2cm). Assuming that a tolerable droop in the output voltage in this time is 1%, then:

$$e^{\frac{-4\text{x}10^{-4}}{\tau_L}} \geqslant 0.99$$

And thus: $\tau_L \geqslant 40$ msec.

3.4 Noise

The minimum expected charge of 10^{-14} coulombs corresponds to $62.5\text{x}10^{4}$ electronic charges. Therefore to keep the error in the output signal less than 10%, the equivalent noise charge, N (defined in Chapter 4), should be less than 6000 electronic charges. Since the charge and velocity measurements are obtained from oscilloscope traces, where the measurement accuracy is about 5%, a 10% error in the worst case charge measurement is assumed to be acceptable.

3.5 Feedback Capacitor

The feedback capacitance affects much of the amplifier performance and the choice of C_F must, in the final analysis, be a compromise. It is desirable to have C_F "large" for accurate determination of the applied charge, high closed loop frequency response (less gain), and accurate knowledge

of the value of C_F itself. It is desirable to have C_F "small" for large closed loop gain (less bandwidth) and small equivalent noise charge.

An estimate of the value of C_F can be obtained. For an applied step of charge Q the charge at the amplifier input is:

$$Q_A = \frac{C_A+(1+A)C_F}{C_D+C_A+(1+A)C_F}\,Q \qquad (3.1)$$

In Chapter 4 the input noise charge is given by:

$$Q_n = C_t\overline{n} \qquad (4.16)$$

where: $\overline{n}$ is the equivalent input rms noise voltage

and $C_t = C_A + C_D + C_F$.

The capacitance C_D is a property of the detection system and was measured and found to be about 50 pf for the four detectors and their interconnectors. The amplifier input capacitance should be small, and an input capacitance of less than 10 pf can be readily achieved with a MOSFET. Further, it is assumed that an open loop gain of at least 5000 is realizable.

If C_F is greater than 1 pf then the applied charge can be measured to an accuracy of 1%. Thus noise will determine the system accuracy when the particles have little charge.

The thermal and 1/f noise contributions to the noise charge are proportional to C_t, while the leakage noise contribution is inversely proportional to C_t. This is shown in Chapter 4. Since the leakage contribution to noise is small for a MOSFET, C_F should be less than $C_D + C_A$ in order that C_F does not significantly contribute to the total noise charge. An increase in C_t of less than 10% will change the worst case charge measurement accuracy to about 11%. Larger increases in C_t are undesirable and so C_F should be less than 6 pf.

3.6 Environmental Conditions

If the amplifier is connected directly to the detection system, the detector capacitance and hence the equivalent noise charge is kept to a minimum since cables to the amplifier input are not required. Also, the "pick-up" of extraneous signals is reduced. This direct connection requires the amplifier to operate in the vacuum system. Thus power dissipation must be kept to a minimum since the removal of heat by convection is not possible in a vacuum. Further, the physical size of the amplifier is limited.

If further amplification is necessary it is proposed to do this outside the vacuum using low-noise post amplifiers.

3.7 Summary of Amplifier Requirements

1. Closed loop upper corner frequency; $f_H \geq 875$ KHz.
2. Hold time constant; $\tau_L \geq 40$ msec.
3. Open loop gain; $-A \geq 5000$.
4. Equivalent noise charge; $N \leq 6000$ electronic charges.
5. Feedback capacitor; $1.0 \text{ pf} \leq C_F \leq 6.0$ pf.

IV CHARGE-SENSITIVE AMPLIFIER NOISE

The minimum signal that can be accurately measured is determined by the noise level of an amplifier. Therefore it is constructive to be able to estimate the expected noise. Of the many ways of expressing noise, a wideband equivalent input noise voltage gives the best indication of the smallest discernible signal. For a charge-sensitive amplifier this voltage can be readily converted into an equivalent noise charge.

4.1 Noise Representation

Although noise is generated throughout a physical system, its effect at the output is independent of its origin. Thus all noise can be referred to the input of the system. Furthermore, in an amplifier, it is the noise of the first stage that generally dominates as it sees the full power gain of the amplifier. This is evident from Equation 4.1.(13)

$$F_T = F_1 + \frac{F_2 - 1}{G_1} + \frac{F_3 - 1}{G_1 G_2} + \cdots \qquad (4.1)$$

where: F_i is the noise factor of the i^{th} stage

and G_i is the power gain of the i^{th} stage.

Therefore the expected noise can usually be estimated by considering only the noise contribution of the source and the input device.

The noise in any active two-port can be described by four noise parameters.(14) The two generator model is particularly convenient to use for reactive sources. The parameters are two noise generators ($\bar{e}_n$ and $\bar{i}_n$ in Figure 4.1) and their complex correlation (γ in Figure 4.1).(15)

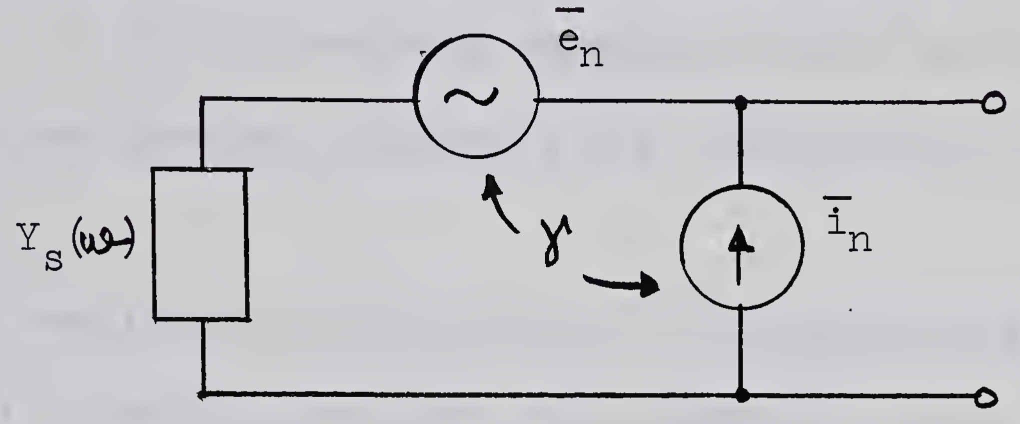

FIGURE 4.1 TWO GENERATOR MODEL OF NOISE

4.2 Noise in Feedback Amplifiers

It is often stated that feedback does not alter the signal-to-noise ratio of an amplifier since both the signal and the noise are reduced by the same factor. However, Van der Ziel(16) points out that care must be exercised when applying this statement to many systems. It is more accurate to say: If, in an amplifier with output voltage (current) feedback, the output load impedance is short circuited (open circuited) for signal frequencies, a new amplifier without

[illegible]

[illegible]

[illegible]

[illegible]

feedback is obtained. The spot noise figure of the new amplifier is the same as that of the feedback amplifier from which it was obtained.

Thus, for the charge-sensitive amplifier, the proper $\overline{e}_n$, $\overline{i}_n$, and noise-input admittance can be obtained by removing the voltage feedback loop from its output and grounding it. As a result, it is the feedback impedance itself and not the Miller-effected feedback impedance that determines the noise properties.

Signal resolution is determined by wideband noise. Hence the spectral intensity, the per unit bandwidth noise, of the instantaneous noise must be integrated over the frequency response to give an accurate representation of the effects of noise. For a feedback amplifier the frequency response used must be the closed loop frequency response.

4.3 MOSFET Noise

Relatively few papers have been published about the noise of MOS-devices and most manufacturers are somewhat unwilling to cite noise characteristics. However, at present, the 1/f noise of MOSFETs is excessive, with the 1/f noise power turnover frequency as high as a few tens of megahertz.(17) (The results of the experimental determination of this frequency are given in Appendix III.)

Jordan and Jordan(18) indicate that, for frequencies at which the excess noise is small, MOSFETs are similar to junction FETs from a noise point of view. Thus the theory of Van der Ziel(19,20) may be applied. Jordan and Jordan attribute noise at the gate of MOSFETs to fluctuations in the occupation of surface states which modulate the channel conductance and result in noise that is 1/f in character, shot noise, and leakage noise. They include as other noise sources: thermal noise generated in the conducting channel, thermal noise generated in the bulk source and drain resistances, and generation-recombination noise which is 1/f in character.

In junction FETs above the 1/f corner frequency the thermal noise generated in the active channel dominates. It is expected that this will be even truer for MOSFETs as their gate leakage is much smaller. Van der Ziel shows that the thermal noise generated in the conducting channel is proportional to the transconductance of the device.

To estimate the noise of MOSFETs it is assumed that the thermal noise generated in the bulk resistances can be neglected and that all the 1/f noise can be combined with the thermal noise of the conducting channel. This noise can then be referred to the input of the device as a voltage noise generator. The remaining gate noise sources are lumped into an

equivalent current noise generator. This results in the representation Sevin(21,22) gives for the two generator model of junction FET noise. For field-effect devices at frequencies below 10 MHz the generators can be considered uncorrelated. Therefore γ is zero, and the spectral intensities can be defined:

$$P_e = \overline{e_n}^2/df \tag{4.2}$$

$$\text{and } P_i = \overline{i_n}^2/df \tag{4.3}$$

Sevin's current generator is:

$$\overline{i_n}^2 \simeq \overline{i_{sh}}^2 = 2qI_{GSX}df \tag{4.4}$$

where: i_{sh} is the shot noise of the gate leakage current.

I_{GSX} is the biased static gate current

and q is the electron charge ($1.6\text{x}10^{-19}$coul).

Therefore the spectral intensity is:

$$P_i = 2qI_{GSX} \tag{4.5}$$

Now P_e represents two sources; one frequency independent (white noise) and the other inversely proportional to frequency (1/f noise). In obtaining the equivalent wideband input noise it is convenient to separate these sources.

Then:

$$P_e = P_w + \frac{P_f}{\omega} \qquad (4.6)$$

Sevin's voltage generator is:

$$\overline{e}_n^{\,2} = \frac{4kT}{y_{fs}} \left(1 + \frac{\omega_{CF}}{\omega}\right) \qquad (4.7)$$

where: y_{fs} is the device transconductance

$f_{CF} = \omega_{CF}/2\pi$ is the noise-power corner frequency

k is Boltzmann's constant (1.38×10^{-23} joules/^{o}K)

and T is the absolute temperature (^{o}K).

Therefore the spectral intensities are:

$$P_w = \frac{4kT}{y_{fs}} \quad ; \quad P_f = \frac{4kT\omega_{CF}}{y_{fs}} \qquad (4.8)$$

Van der Ziel modifies Equation 4.7 by a slowly varying multiplicative factor which reduces the value of $\overline{e}_n^{\,2}$. This factor is generally between 0.6 and 0.67.(23)

4.4 Wideband Noise

Figure 4.2 shows the noise model of the source and the input device of the charge-sensitive amplifier. Detector leakage resistance and the input resistance of the MOSFET are omitted in the analysis since both are extremely large. The thermal noise of the gate-bias resistor, which for the charge-sensitive amplifier is the feedback resistor R_F (not

$R_F/(1+A)$), is converted into a noise current, i_b, with spectral intensity $P_b = 4kT/R_F$. The two current generators may be combined to give a spectral intensity P_p.

$$P_p = 2qI_p \tag{4.9}$$

where: $I_p = I_{GSX} + 4kT/2qR_F$

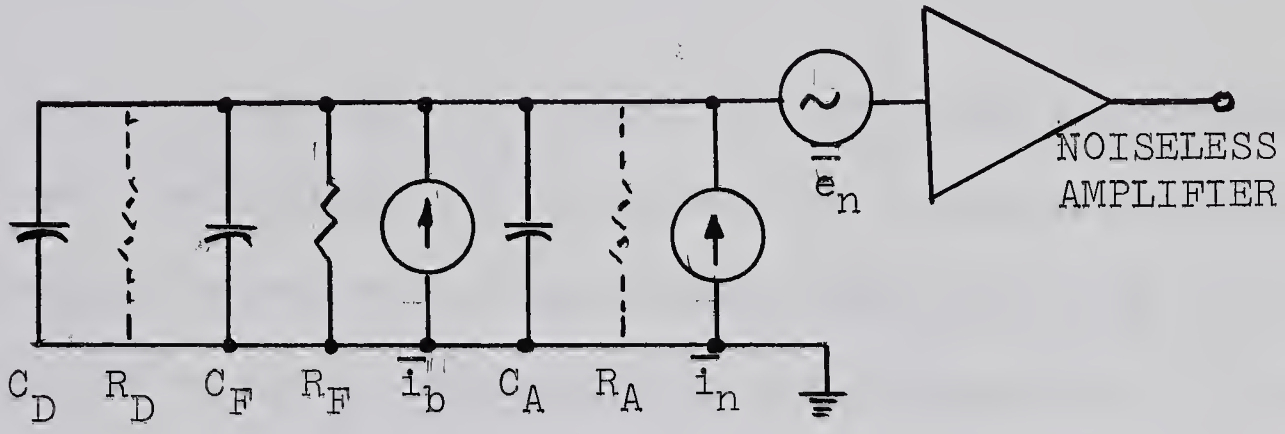

FIGURE 4.2 NOISE MODEL OF A CHARGE-SENSITIVE AMPLIFIER

Since, for MOSFETs, I_{GSX} is extremely small; R_F must be very large if it is not to significantly contribute to the over-all leakage noise.

It can be assumed, for the system to be used, that the closed loop frequency response of the amplifier determines the system pass-band. From Chapter 2 the closed loop frequency response is:

$$|G(\omega)|^2 = A_c^2 a^2 \omega_H^4 \frac{\omega^2}{(\omega_L^2+\omega^2)(\omega_H^2+\omega^2)(a^2\omega_H^2+\omega^2)} \tag{4.10}$$

The equivalent rms input noise voltage, $\overline{n}$, can now be found. From Figure 4.2:

$$\overline{n}^2 = \frac{1}{A_c^2} \int_0^\infty \left\{ P_w \left| G(\omega) \right|^2 + \frac{P_f}{\omega} \left| G(\omega) \right|^2 + P_p \left| \frac{G(\omega)}{Y_t(\omega)} \right|^2 \right\} \frac{d\omega}{2\pi} \qquad (4.11)$$

where: $Y_t(\omega)$ is the total source and noise-input admittance.

For a charge-sensitive amplifier the source resistance, the input resistance, and the effective noise-bias resistance are large; therefore the input-source admittance can be considered to be purely capacitive at the frequencies of interest.

$$\left| Y_t(\omega) \right|^2 = \frac{1+\omega^2 R_t^2 C_t^2}{R_t^2} \simeq \omega^2 C_t^2 \qquad (4.12)$$

where: $C_t = C_D + C_A + C_F$

Then:

$$\overline{n}^2 = P_w I_1 + P_f I_2 + \frac{P_p}{C_t^2} I_3 \qquad (4.13)$$

where, letting $D(\omega) = (\omega_L^2+\omega^2)(\omega_H^2+\omega^2)(a^2\omega_H^2+\omega^2)$:

$$I_1 = \frac{a^2\omega_H^4}{2\pi} \int_0^\infty \frac{\omega^2}{D(\omega)} \, d\omega$$

$$I_2 = \frac{a^2\omega_H^4}{2\pi} \int_0^\infty \frac{1}{D(\omega)} \omega \, d\omega$$

[illegible]

$$[illegible]$$

[illegible]

[illegible]

$$[illegible]$$

[illegible]

[illegible]

$$[illegible]$$

[illegible]

$$[illegible]$$

$$[illegible]$$

and $$I_3 = \frac{a^2\omega_H^4}{2\pi}\int_0^\infty \frac{1}{D(\omega)}\,d\omega$$

The integrals can be evaluated easily using partial fraction expansions. For the case of I_2 the ω in the numerator is grouped with the $d\omega$ so that the Heavyside coefficients are all real.

Upon integration:

$$I_1 = \frac{1}{4}\,\frac{a^2}{a+1}\,\frac{\omega_H^3}{(\omega_H+\omega_L)(a\omega_H+\omega_L)}$$

$$I_2 = \frac{1}{2\pi}\,\frac{a^2}{a^2-1}\,\frac{\omega_H^2}{(\omega_H^2-\omega_L^2)(a^2\omega_H^2-\omega_L^2)}\left[a^2\omega_H^2\ln\frac{\omega_H}{\omega_L} + \omega_L^2\ln a + \omega_H^2\ln\frac{\omega_L}{a\omega_H}\right]$$

$$I_3 = \frac{1}{4}\,\frac{a}{a+1}\,\frac{\omega_H}{\omega_L}\,\frac{\omega_H+a\omega_H+\omega_L}{(\omega_H+\omega_L)(a\omega_H+\omega_L)} \qquad (4.14a)$$

For a wideband charge-sensitive amplifier $\omega_H \gg \omega_L$, and the integrals may be approximated by:

$$I_1 = \frac{1}{4}\,\frac{a}{a+1}\,\omega_H$$

$$I_2 = \frac{1}{2\pi(a^2-1)}\left[a^2\ln\frac{\omega_H}{\omega_L} + \ln\frac{\omega_L}{a\omega_H}\right]$$

$$I_3 = \frac{1}{4}\,\frac{1}{\omega_L} \qquad (4.14b)$$

4.5 Equivalent Input Noise Charge

Since charge is the quantity that is to be measured it is appropriate to define noise on a charge basis. An equivalent input noise charge, Q_n, can be defined as:(24)

> That quantity of charge which when applied instantaneously to the amplifier input produces an output pulse of amplitude equal to the root mean square output noise voltage.

Then:

$$Q_n = \frac{C_t \bar{n}}{S} \quad \text{coulombs} \qquad (4.15)$$

where: S is the peak output signal in response to a unit step input signal over the input.

For a wideband system, S is very nearly unity.

Then:

$$Q_n = C_t \bar{n} \quad \text{coulombs} \qquad (4.16)$$

Q_n is generally expressed in the number of electronic charges that are equivalent to the rms noise.

Thus:

$$N = \frac{Q_n}{q} \qquad (4.17)$$

Q_n can also be expressed in particle energy units, and is usually so expressed in nuclear work.

V AMPLIFIER DESIGN

5.1 Proposed Amplifier

The proposed amplifier is of conventional design, with some modifications made in an attempt to increase the open loop gain without adversely affecting either the frequency response or the noise performance. The amplifier is shown in Figure 5.1.

An input cascode with a large dynamic load affords high gain and input isolation in a simple stage. Rather than using "bootstrapping"(25,26,27,28) or positive current feedback(29,30) to increase the dynamic load of the cascode, a transistor current source is used. The bootstrapping technique reduces the low frequency gain and requires large capacitors, while positive current feedback often leads to instabilities. The transistor current source allows the d-c conditions to be met with reasonable power supply voltages, and yet presents a large a-c impedance to the cascode. To increase the effective transconductance, y_{fs}, of the MOSFET, it is compounded with a junction transistor. An emitter follower output stage prevents loading of the cascode and provides a low output impedance.

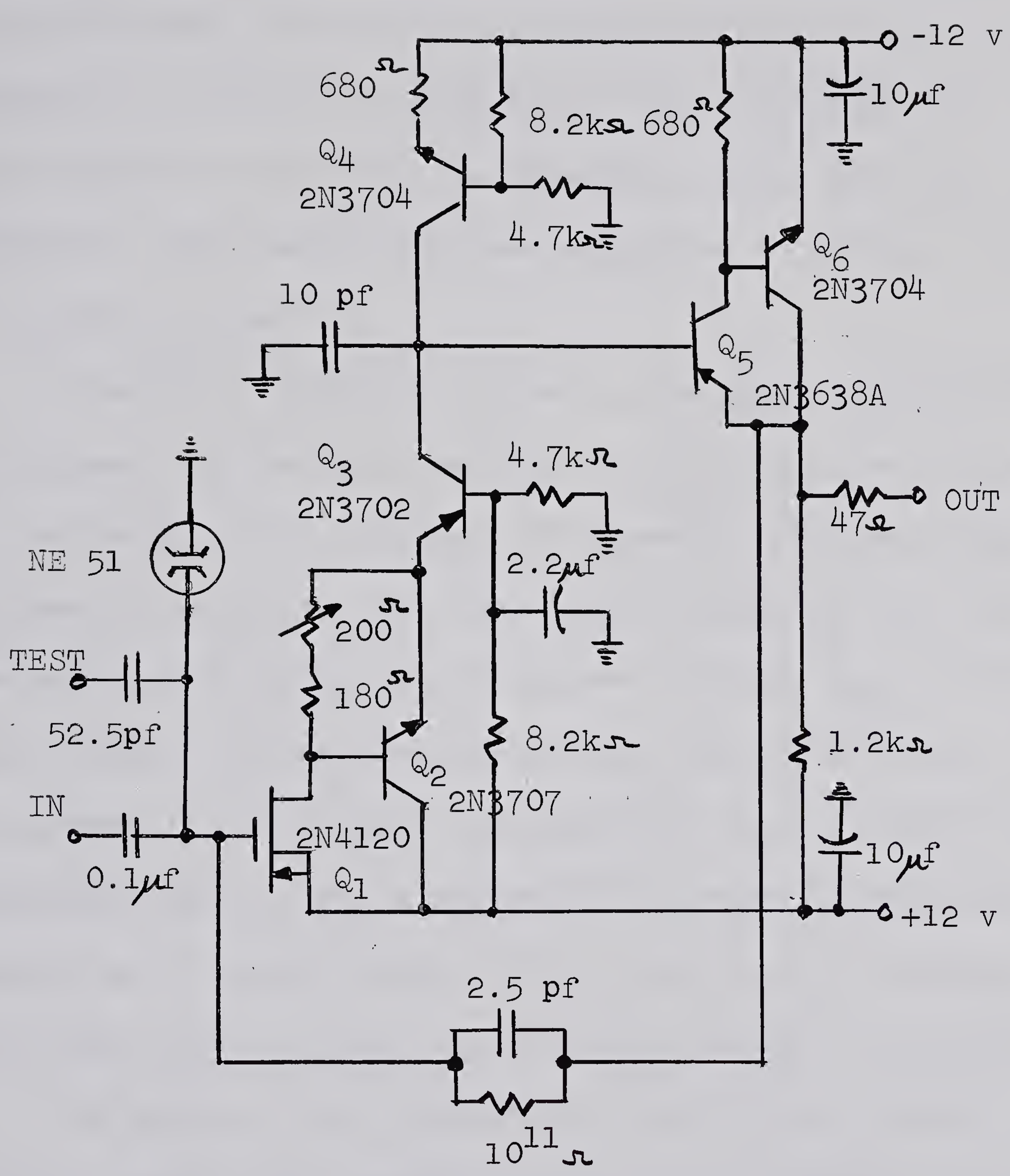

FIGURE 5.1 CHARGE-SENSITIVE AMPLIFIER

5.2 Quiescent Conditions

A split supply of ± 12 volts was chosen. This allows the d-c potential of the input and the output to be nominally zero volts. Further, 24 volts allows adequate operating voltages across the "column" of three active devices. Operating currents should be high for low impedance levels and thus, since parasitic capacitances are less sensitive to current levels, for greater bandwidth.

A Fairchild 2N4120 P-channel, enhancement mode MOSFET was chosen for the input device, Q_1. The 2N4120 was chosen on the basis of its stability of operating parameters and the uniformity among devices. For a gate voltage of zero volts the maximum available gate-to-source voltage, V_{GS}, is -12 volts. Then, for the devices on hand, the drain current, I_D, is between 1.5 and 3 ma. The transistor, Q_2, in compound with the MOSFET should, for a reasonable increase in over-all y_{fs}, operate at a current greater than I_D and have a large h_{fe}. The total column current was therefore chosen to be 10 ma.

The bases of the transistor in the current source, Q_4, and the common base transistor, Q_3, of the cascode are biased at $-V_B$ and $+V_B$ respectively. The collector-to-emitter voltages of Q_4 and Q_3 were chosen to be about four volts to allow sufficient voltage across the MOSFET to bias it in the linear

pinch-off region ($|V_{DS}| \geq 6$ volts for $V_{GS} = -12$ volts). Therefore a V_B of 4.7 volts is necessary.

A complementary compound is used for the emitter follower to obtain a very high input impedance and a low output impedance. The emitter follower current was chosen to be 10 ma, with Q_5 operating at 1 ma and Q_6 operating at 9 ma and the V_{CE}'s about 12 volts.

5.3 Small Signal Analysis

In the following analysis it is assumed that the frequency is such that the by-pass capacitors can be considered to be short circuits and the parasitic capacitances open circuits.

5.3.1 Output Stage

The output stage is shown in Figure 5.2. For their operating points the mixed h-parameters of Q_5 and Q_6 are:

Q_5	Q_6
$h_{ib5} = 30$ ohms	$h_{ib6} = 5$ ohms
$h_{fe5} = 150$	$h_{fe6} = 300$
$h_{rb5} = 3\text{x}10^{-4}$	$h_{rb6} = 4\text{x}10^{-4}$
$h_{ob5} = 0.4\text{x}10^{-6}$ mhos	$h_{ob6} = 0.5\text{x}10^{-6}$ mhos

The h_{fe}'s, h_{rb}'s, and h_{ob}'s were measured; while the h_{ib}'s

were found from the familiar diode-equation-derived expression:

$$h_{ib} = \frac{26\text{mv}}{I_E} + 1.5 \quad \text{ohms} \tag{5.1}$$

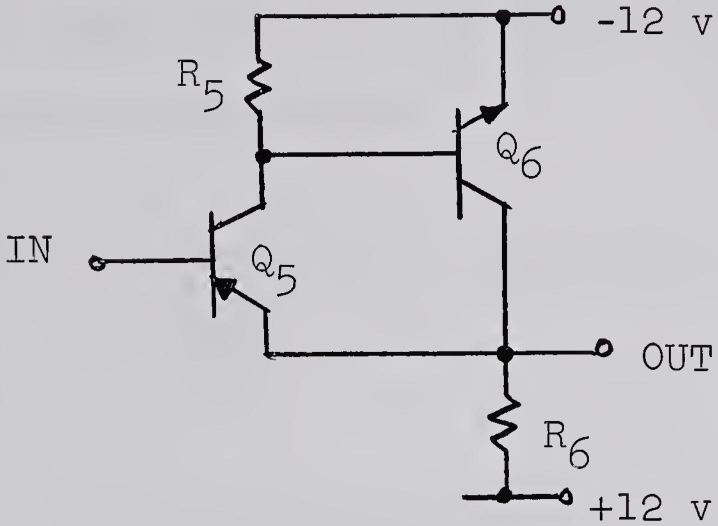

FIGURE 5.2 OUTPUT STAGE

The compound is conventional and after R_5 is lumped with Q_6 to form Q_6' the equations of Edwards$^{(31)}$ hold and the compound can be considered as a single PNP transistor, Q_5*. Since $h_{ib6}/R_5 \ll 1$, the h'-parameters, as tabulated in Appendix II, can be approximated by:

$$h_{ib6}' \simeq h_{ib6} = 5 \text{ ohms} \qquad h_{rb6}' \simeq h_{rb6} = 4\text{x}10^{-4}$$

$$h_{fe6}' \simeq h_{fe6} \frac{1}{1+\frac{h_{fe6}h_{ib6}}{R_5}} = 94 \qquad h_{ob6}' \simeq h_{ob6} + \frac{h_{rb6}}{R_5} = 1.1\text{x}10^{-6}\text{mhos}$$

Edward's equivalent single transistor equations (tabulated

[illegible]

[illegible]

[illegible]

in Appendix II) yield:

$h_{ib5}^* \simeq 0.32$ ohms $\qquad h_{rb5}^* \simeq 3.3\text{x}10^{-4}$

$h_{fe5}^* \simeq 14{,}000 \qquad h_{ob5}^* \simeq 0.4\text{x}10^{-6}$ mhos

The voltage gain and input impedance of the emitter follower can now be calculated.

$$A_{vc5}^* = \frac{1 - h_{rb5}^*}{1 + \frac{h_{ib5}^*}{R_6}} = 1 - 6\text{x}10^{-4} \simeq 1$$

$$Z_{ic5}^* = \frac{h_{fe5}^*(h_{ib5}^* + R_6)}{1 + h_{fe5}^* h_{ob5}^* R_6} \simeq \frac{1}{h_{ob5}^*} = 2.27 \text{ MOhms}$$

Therefore the emitter follower will cause no appreciable signal loss and will not adversely load the current source.

5.3.2 Current Source

The current source is shown in Figure 5.3. The purpose of C_L is discussed in Section 5.7.

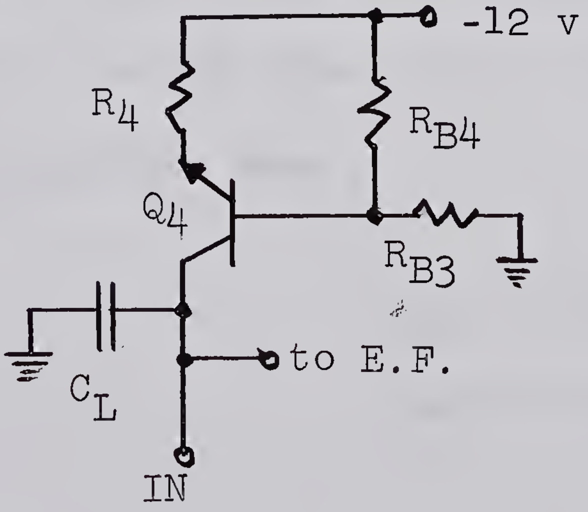

FIGURE 5.3 CURRENT SOURCE

The mixed h-parameters for Q_4 at its operating point are:

$h_{ib4} = 4$ ohms $\qquad h_{rb4} = 1\times10^{-4}$

$h_{fe4} = 300 \qquad h_{ob4} = 0.25\times10^{-6}$ mhos

R_4 is lumped with Q_4 to yield an equivalent transistor, Q_4'. From Appendix II and since $h_{fe4}h_{ob4}R_4 \ll 1$, the approximate mixed h'-parameters are:

$h_{ib4}' \simeq h_{ib4} + R_4 = 684$ ohms $\qquad h_{rb4}' \simeq h_{rb4} = 1\times10^{-4}$

$h_{fe4}' \simeq h_{fe4} = 300 \qquad h_{ob4}' \simeq h_{ob4} = 0.25\times10^{-6}$ mhos

Only the output admittance is of concern and is:

$$Y_{oe4}' = h_{ob4}' + \frac{h_{ob4}'R_B + h_{rb4}'}{h_{ib4}' + \frac{R_B}{h_{fe4}'}} \simeq h_{ob4}'\left(1 + \frac{R_B}{R_4}\right) = 1.4\times10^{-6} \text{ mhos}$$

where: $R_B = R_{B3}//R_{B4}$

5.3.3 Common Base Stage

The common base stage is shown in Figure 5.4. The load Z_L is $Z_{oe4}'//Z_{ic5}^*$ and is 560 KOhms. The mixed h-parameters of Q_3 at its operating point are:

$h_{ib3} = 4$ ohms $\qquad h_{rb3} = 4\times10^{-4}$

$h_{fe3} = 200 \qquad h_{ob3} = 0.5\times10^{-6}$ mhos

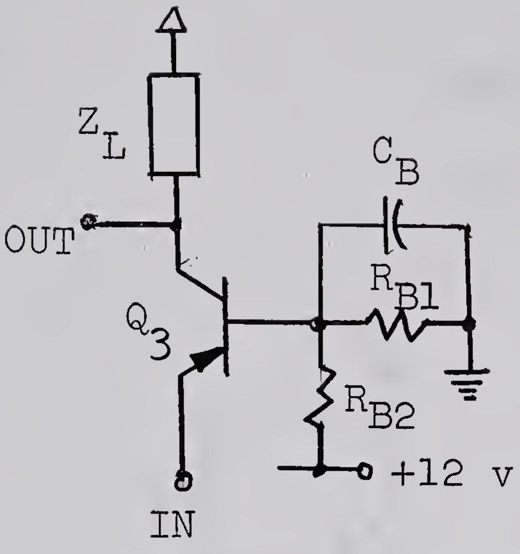

FIGURE 5.4 COMMON BASE STAGE

Assuming the base resistance to be by-passed the voltage gain is:

$$A_{vb3} = \frac{Z_L}{h_{ib3}} \frac{1}{1 + (h_{ob3} h_{ib3} + h_{rb3}) \frac{Z_L}{h_{ib3}}} \simeq \frac{1}{h_{rb3}} = 2500$$

And the input impedance is:

$$Z_{ib3} = h_{ib3} + \frac{h_{rb3} Z_L}{1 + h_{ob3} Z_L} = 185 \text{ ohms}$$

5.3.4 Input Stage

The MOSFET compound input stage is shown in Figure 5.5. For Q_1, the MOSFET, only the transconductance and the output conductance are of interest; and they were measured and found to be:

$y_{fs1} = 700 \times 10^{-6}$ mhos $\qquad$ $y_{os1} = 40 \times 10^{-6}$ mhos

The mixed h-parameters for Q_2 are:

$h_{ib2} = 5$ ohms $\qquad h_{rb2} = 2\text{x}10^{-4}$

$h_{fe2} = 250 \qquad h_{ob2} = 0.2\text{x}10^{-6}$ mhos

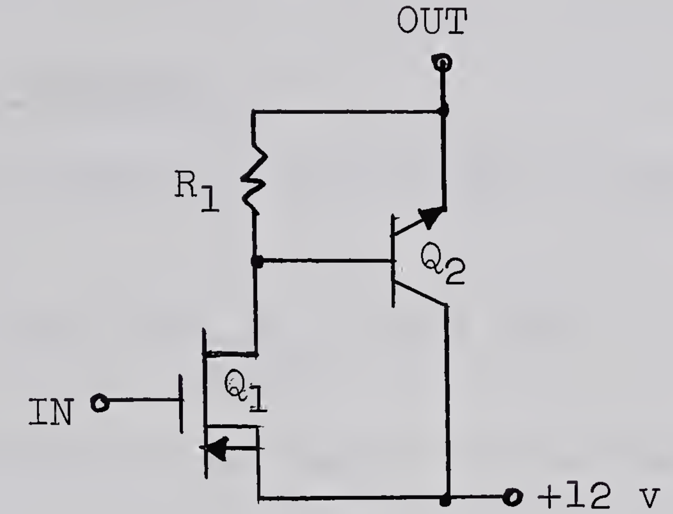

FIGURE 5.5 INPUT STAGE

Using the h'-parameters tabulated in Appendix II to lump R_1 (approximately 300 ohms) with Q_2 to form Q_2' results in (since $h_{ib2}/R_1 \ll 1$):

$$h_{ib2}' \simeq h_{ib2} = 5 \text{ ohms} \qquad h_{rb2}' \simeq h_{rb2} = 2\text{x}10^{-4}$$

$$h_{fe2}' \simeq h_{fe2}\frac{1}{1+\frac{h_{fe2}h_{ib2}}{R_1}} = 48.5 \qquad h_{ob2}' \simeq h_{ob2} = 0.2\text{x}10^{-6} \text{ mhos}$$

Since $y_{os1}h_{ib2}'h_{fe2}' \ll 1$ and since $h_{ob2}' \ll y_{os1}$, the equivalent MOSFET equations of Appendix II give:

$$y_{fs1}^* \simeq h_{fe2}'y_{fs1} = 34\text{x}10^{-3} \text{ mhos}$$

$$y_{os1}^* \simeq h_{fe2}'y_{os1} = 19.4\text{x}10^{-4} \text{ mhos}$$

Therefore the voltage gain of the input stage is:

$$A_{vs1}^* = - \frac{y_{fs1}^* Z_{ib3}}{1 + Z_{ib3} y_{os1}^*} = -4.6$$

Thus the total expected open loop gain is, $A_T = -11{,}500$.

5.3.5 Output Impedance

The output impedance of the input stage is:

$$Z_{os1}^* \simeq \frac{1}{y_{os1}^*} = 515 \text{ ohms}$$

And hence, the output admittance of the common base stage is:

$$Y_{ob3} \simeq h_{ob3} + \frac{h_{rb3}}{h_{ib3} + Z_{os1}^*} = 1.3\text{x}10^{-6} \text{ mhos}$$

The admittance seen by the base of the emitter follower is $Y_{ob3} + Y_{oe4}'$, therefore the impedance is $Z_{s5}^* = 380$ KOhms. The amplifier output impedance is then:

$$Z_{oc5}^* = \frac{h_{ib5}^* + Z_{s5}^*/h_{fe5}^*}{1 + h_{ob5}^* Z_{s5}^*} = 24 \text{ ohms}$$

This value is sufficiently small to prevent loading of the amplifier by succeeding stages.

5.4 Frequency Response

The low frequency response will be governed by C_B. When $R_{B1}//R_{B2}$ is not by-passed, the effective h_{rb3}' is increased

and so the common base gain is lowered. However, the input impedance of the common base stage is increased and therefore the gain of the input stage increases. Thus, for low frequencies, the open loop gain remains about the same. This means that the d-c feedback is large and consequently amplifier drift should be minimized. By-passing $R_{B1}//R_{B2}$ also reduces r_{bb3}' and hence the noise contribution of the common base stage. As well, since the gain of the input stage is smaller when $R_{B1}//R_{B2}$ is by-passed; the Miller-effected gate-to-drain capacitance at the amplifier input is smaller. This is desirable from a noise point of view.

C_L, the various C_{ob}'s, and the frequency dependence of h_{rb3} all cause the gain to fall off at high frequencies. An equation can be derived for the total frequency dependent gain:

$$A_T(\omega) = \frac{-y_{fs1}^*}{\{Y_L(\omega)+H_{ob3}(\omega)\}(1+y_{os1}^*h_{ib3}) + y_{os1}^*H_{rb3}(\omega)} \tag{5.2}$$

where:

$$Y_L(\omega) = h_{ob5}+h_{ob4}(1+\frac{R_B}{R_4}) + j\omega\left[C_{ob5}+C_{ob4}(1+\frac{R_B}{R_4})+C_L\right]$$

$$H_{ob3}(\omega) = h_{ob3} + j\omega C_{ob3}$$

$$H_{rb3}(\omega) = h_{rb3} + j\omega K_{rb3}$$

and h_{ib3}, y_{os1}^*, and y_{fs1}^* are assumed to be constant for the frequencies of interest.

Assuming all the C_{ob}'s to be 6 pf and since the h_{rb3} cut-off occurs at 200 KHz, the corner frequency of the open loop gain is expected to be 11 KHz.

The second break frequency is difficult to predict. The output stage cuts off because of the capacity seen by R_6 and because of the increase in h_{ib5}* due to the fall-off of h_{fe6} at high frequencies. The point at which the gain of the emitter follower is down 3 db is estimated to be in the order of 150 MHz.

5.5 Closed Loop Circuit

In Chapter 3 it was shown that C_F should be greater than 1 pf and less than 6 pf. Therefore R_F must be larger than 10^{10} ohms in order to obtain the desired hold time constant. An R_F of 10^{11} ohms was used. The expected leakage current of less than 10^{-13} amp through R_F will not cause a significant offset. A 2.5 picofarad capacitor will give a closed loop gain of about 20 for the expected detector capacitance and was chosen for the feedback capacitor. Thus the expected closed loop lower corner frequency is 0.64 Hz. Or, the hold time constant is expected to be 0.25 seconds.

The closed loop upper corner frequency will not be derived from a staight gain-bandwidth trade, but will depend on the amplifier input capacitance and the detector capacitance.

For $C_A = 10$ pf and $C_D = 50$ pf, the closed loop gain will be down approximately 3 db when the open loop gain is 60, at about 2 MHz. This corresponds to a rise time of 175 ηsec.

5.6 Noise

The noise performance can be estimated using the equations derived in Chapter 4. The gate leakage current of Q_1 is assumed to be less than 10^{-13} amp; otherwise, the device is assumed defective. The 1/f noise corner frequency of the MOSFET was measured and found to be about 30 MHz (see Appendix III). As a result, the 1/f noise term dominates by far the thermal and leakage noise terms.

From:

$$\overline{n}^2 = P_w I_1 + P_f I_2 + \frac{P_p}{C_t^2} I_3 \qquad (4.13)$$

$$P_w I_1 = 2.7\text{x}10^{-10} \text{ volts}^2$$

$$P_f I_2 = 1.5\text{x}10^{-8} \text{ volts}^2$$

$$\frac{P_p}{C_t^2} I_3 = 2.9\text{x}10^{-12} \text{ volts}^2$$

Thus, the expected equivalent input rms noise voltage is 125 μvolts; or, N = 50,000 electronic charges. This is almost ten times the desired noise and limits the smallest charge that can be accurately detected to about 10^{-13} coulombs.

5.7 Practical Considerations

To prevent 60 Hz pick-up at the high impedance input, the amplifier was enclosed in a copper box and coaxial connectors were used at all terminals. The gate of the MOSFET was insulated from the circuit board by Teflon stand-offs.

Transients in excess of 60 volts can puncture the thin silicon dioxide layer at the gate of the MOSFET. In order to prevent puncture, a neon bulb was connected from the gate to ground. Since 1/f noise is so pronounced, the leakage of the neon bulb has negligible effect on the over-all noise. Also, the capacitance of the bulb is small and so does not have a detrimental effect on the amplifier performance.

The 47 ohm resistor at the output of the amplifier, Figure 5.1, acts, with any capacitance added to the output, as a low pass filter. Thus any tendency of the amplifier to oscillate under capacitive loading is reduced. This resistor increases the amplifier output impedance to about 75 ohms. The 10 pf capacitor, C_L, at the output of the common base stage stabilized the amplifier under unity gain closed loop operation.

A photograph of the final amplifier appears as Figure 5.6.

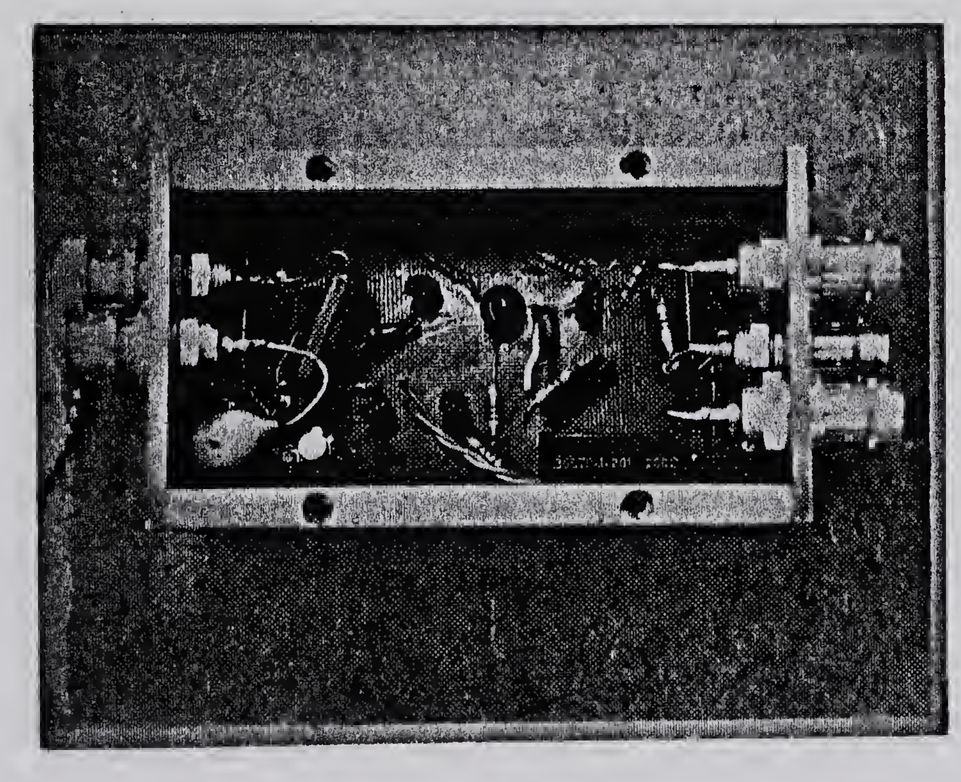

FIGURE 5.6 PHOTOGRAPH OF THE AMPLIFIER

VI AMPLIFIER PERFORMANCE

6.1 Open Loop Response

To measure the open loop response the amplifier was connected as is shown in Figure 6.1. The output and summing-junction voltages were measured. In Figure 6.2 the measured response is compared to the predicted response. Both the low frequency gain and the high frequency roll-off correspond.

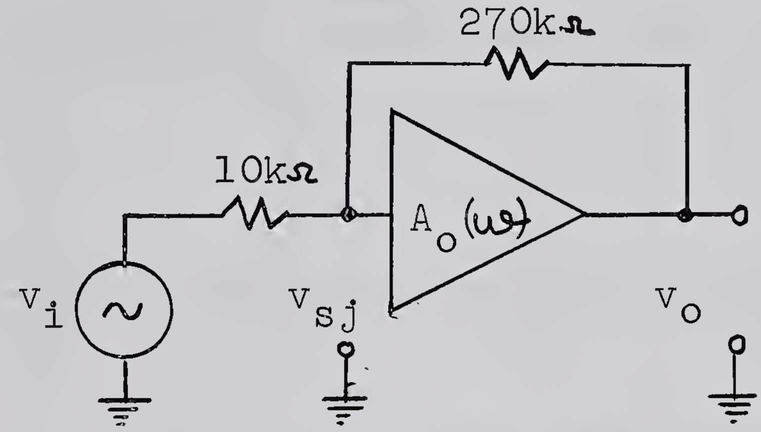

FIGURE 6.1 CONFIGURATION FOR OPEN LOOP RESPONSE

However, the measured response contained a large dip in it. It is thought that this dip is caused by a negative capacitance which arises from the Miller-effected collector-to-emitter capacitance of the common base transistor in the cascode. This capacitance is gain dependent and would initially dominate and then would tend to cancel, at one frequency, with the positive capacitance. This would cause the rise in gain that occurred after the initial drop.

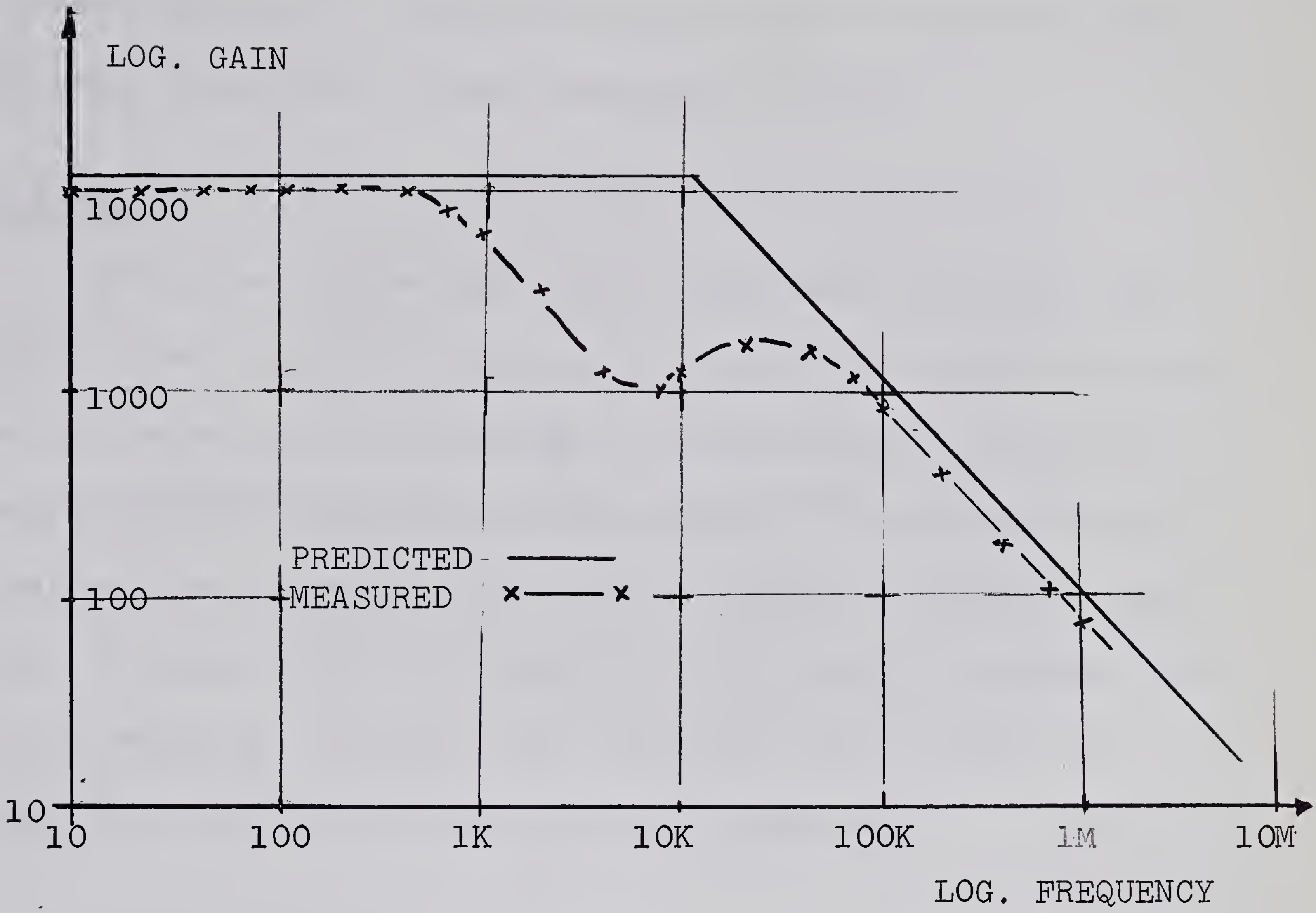

FIGURE 6.2 OPEN LOOP RESPONSE

6.2 Closed Loop Performance

The response of the charge-sensitive amplifier was measured and was found to be flat, within ± 0.3 db, and down 3 db at 0.64 Hz and 2 MHz. The response was measured using the test input, C_D = 52.5 pf. The measured gain was 21.6 which indicates that the total feedback capacitance, including strays, is 2.43 pf. A hold time constant of 0.24 sec and a rise time of 170 η sec were measured. The second high frequency break occurred beyond 10 MHz.

[illegible]

[illegible]

[illegible]

The amplifier was tested using several detector capacitances from 10 pf to 500 pf. When the input charge was kept constant the output voltage remained the same.

6.3 Noise

The noise of the amplifier was measured using the test input. The output rms noise was 3.2 millivolts which indicates an equivalent rms input noise of 148 microvolts. This corresponds to an equivalent noise charge of 55,000 electronic charges. The noise was also passed through a KhronHite bandpass filter and when the ratio of f_H/f_L was kept constant the noise remained the same. This indicates, as is shown in Chapter 4, that the noise is 1/f in character.

6.4 System Performance

A photograph of the amplifier in the vacuum system appears as Figure 6.3. The charging mechanism was operated at several charging voltages and the responses of more than 30 particles were photographed. Figure 6.4 shows the response of a 7 micron-diameter particle traveling at 65 m/sec with a charge-to-mass ratio of 0.19. This particle passed through all the detectors and reached the collector.

Many of the particles were intercepted by the screens. Some of the particles were not properly aligned and were intercepted by the detector cylinders.

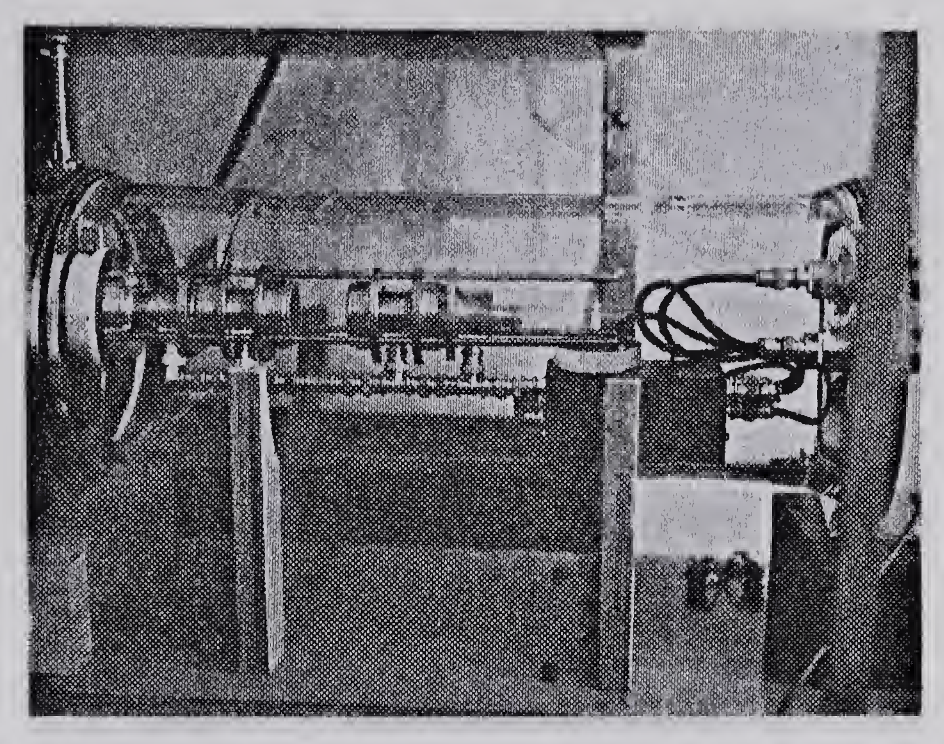

FIGURE 6.3 AMPLIFIER IN SYSTEM

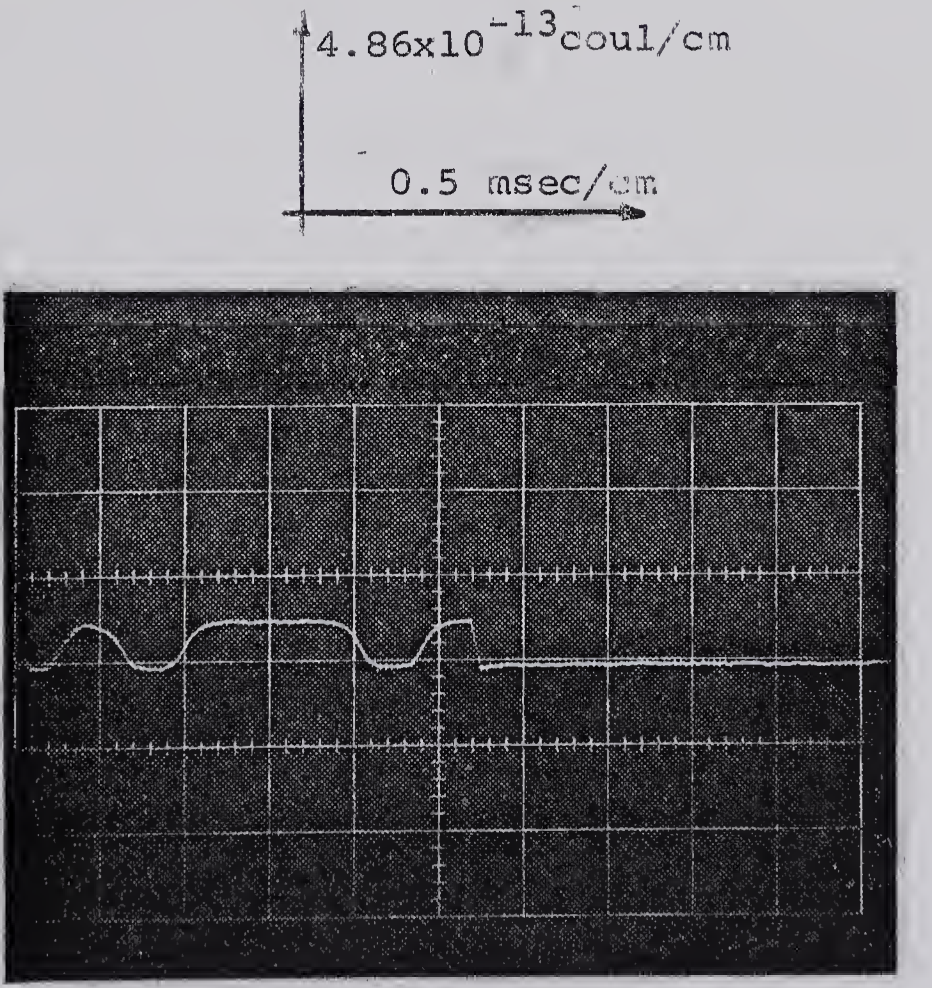

FIGURE 6.4 TYPICAL PARTICLE RESPONSE

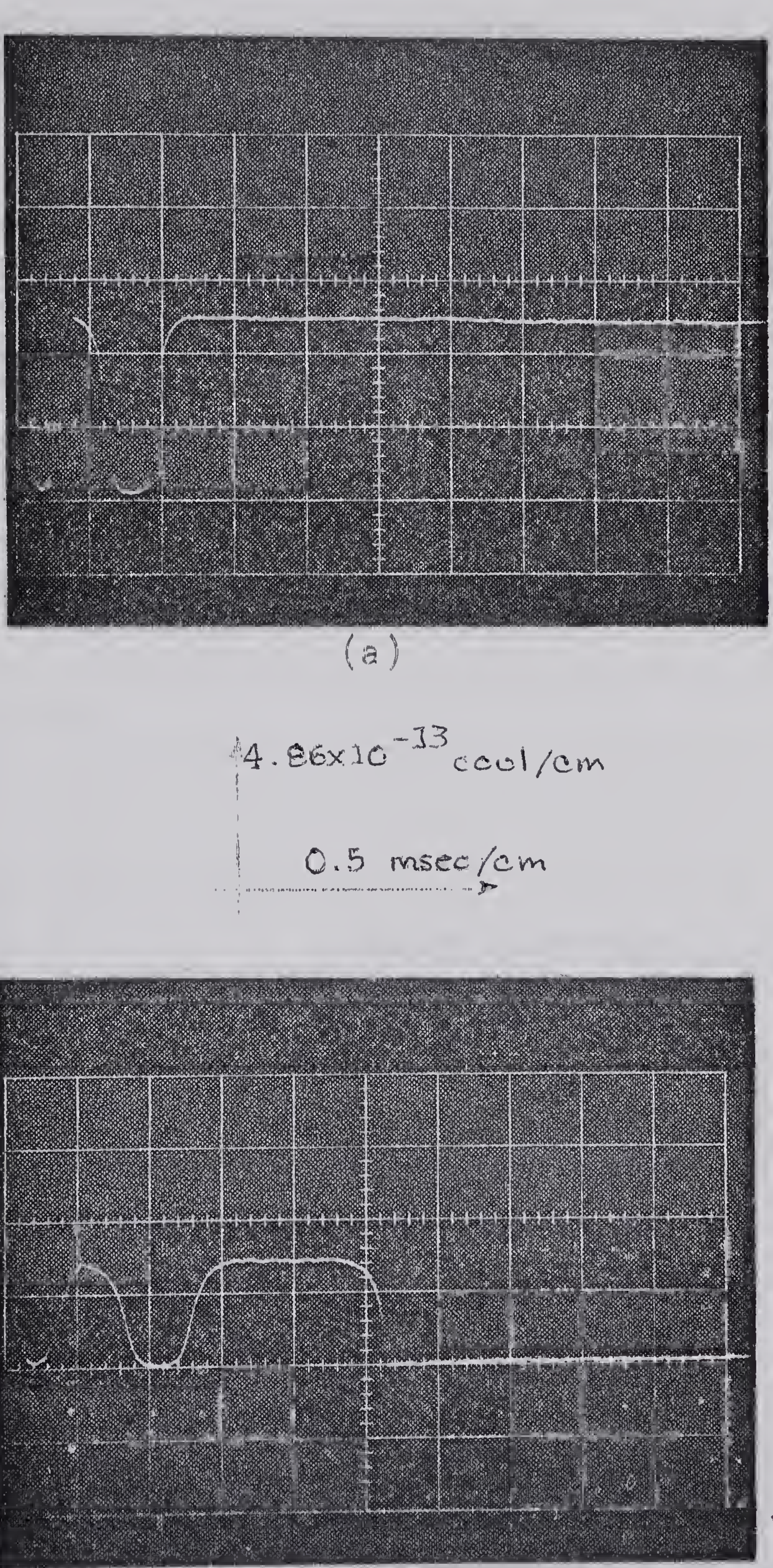

(a)

(b)

FIGURE 6.5 INTERCEPTED PARTICLES

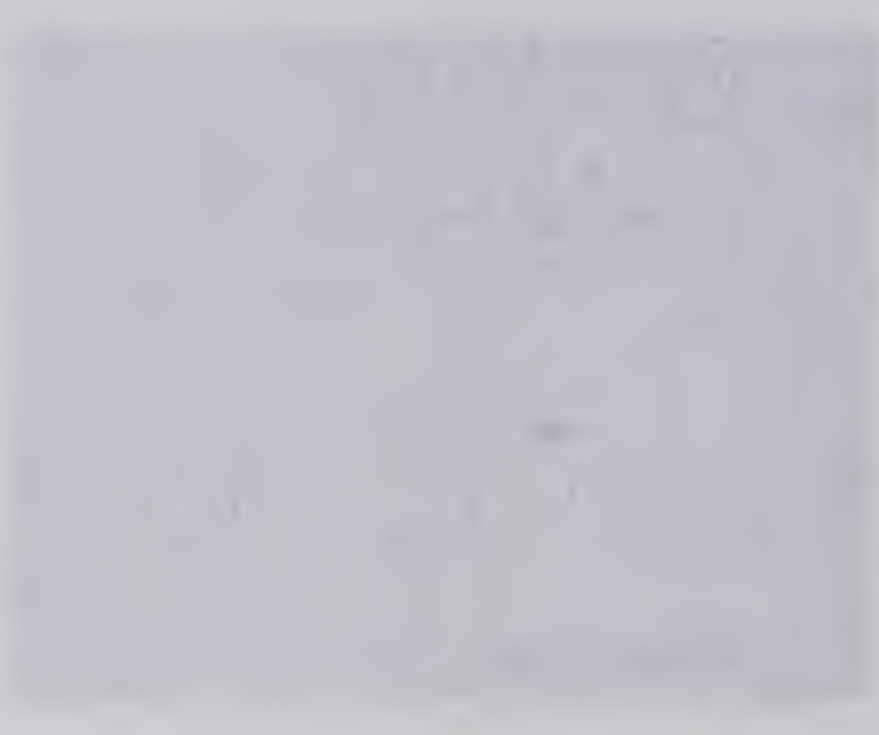

Figure 6.5a shows the response of a particle that was intercepted by the screen at the input of the third detector. Figure 6.5b shows the response of a particle that was intercepted by the cylinder of the third detector.

The theoretical curve of the charge-to-mass ratio versus particle radius for a given charging voltage can be found from Equations 1.2 and 1.3. The radius of the charging sphere was measured and found to be 55 microns. The density of the particles that were used was 7.8×10^3 kg/m^3. Figure 6.6 shows the charge-to-mass ratio curve and some experimental points for a charging voltage of 11 kilovolts.

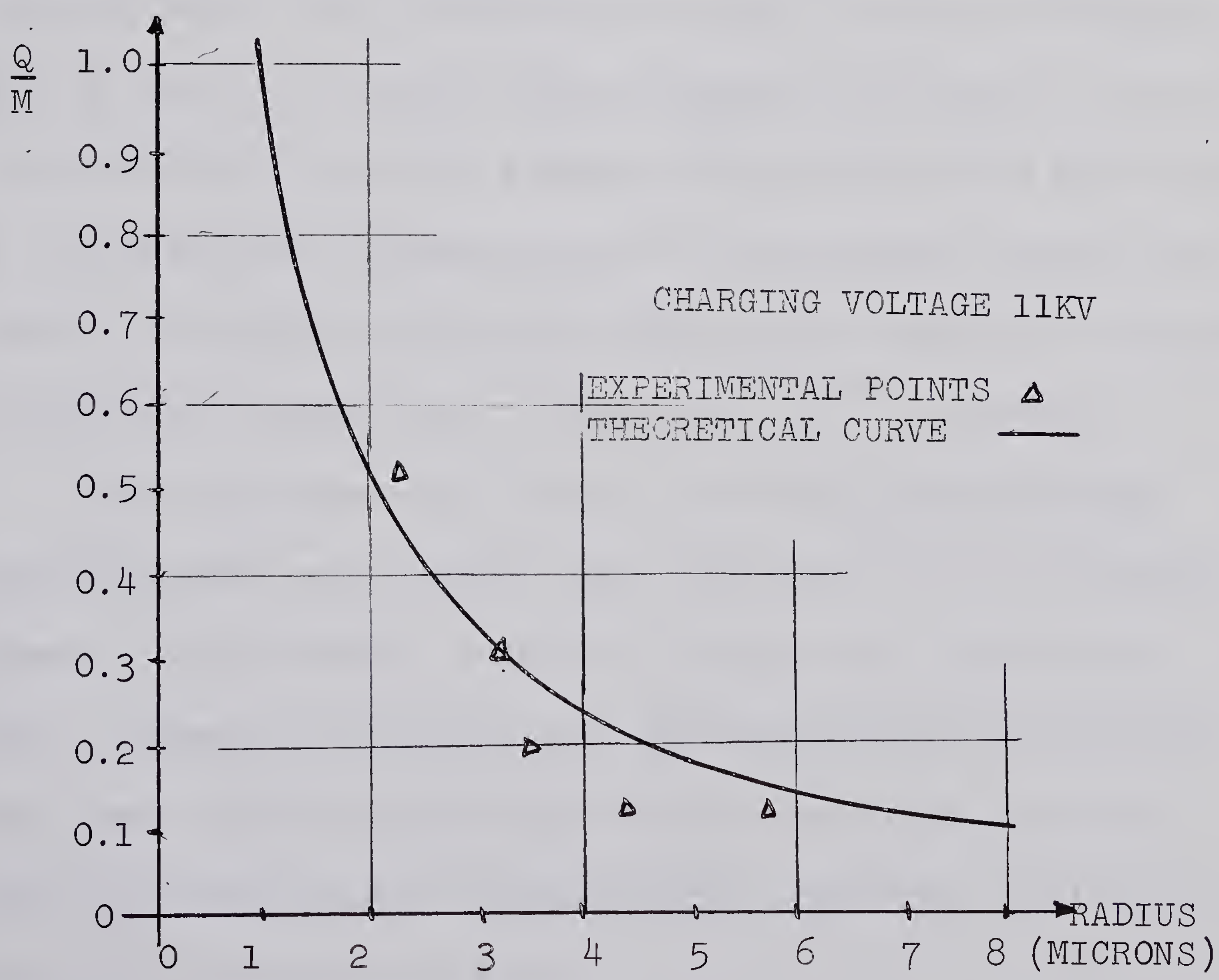

FIGURE 6.6 CHARGE-TO-MASS RATIO VS RADIUS

6.5 Recommendations

Although the amplifier performed satisfactorily, an improvement in the noise level of the amplifier is desirable.

At present, a junction FET could be employed to give a lower noise level. This would require a FET with a gate leakage current of less than 1 ηa, or an increase in the lower corner frequency of the amplifier. FETs with leakage currents of less than a nanoampere are readily available; however, the circuit would have to be completely redesigned in order to obtain the proper biasing.

Since insulated-gate transistors are high frequency devices, since their leakage is so small, and since improvement of their 1/f noise corner frequency is likely; they are better suited for use in wideband charge-sensitive amplifiers. An insulated-gate transistor with a noise-power corner frequency of 300 KHz would enable the present amplifier to detect the smallest charge that is expected (10^{-14} coulombs).

A new insulated-gate device, the Metal-Nitride-Semiconductor FET, has recently been reported.(32,33) The MNSFET appears to have better stability properties, higher breakdown voltages, and better noise performance than the MOSFET. When lower noise insulated-gate FETs become available they can be substituted for the 2N4120 now used with little or no change in the present circuit.

REFERENCES

1) McKinley, D.W.R.: Meteor Science and Engineering, McGraw-Hill Book Co. Inc., New York, p. 126; 1961.

2) Davidson, J.R. and P.E. Sandorff: Environmental Problems of Space Flight Structures-II Meteoroid Hazard, N.A.S.A. Technical Note D-1493, p. 15; Jan. 1963.

3) McKinley, op. cit. 1, p. 126.

4) Wlochowicz, R.: "Detecting Micrometeoroids Acoustically from Rockets", Canadian Journal of Physics, vol. 44, no. 1, pp. 1-25; Jan. 1966.

5) Smythe, W.R.: Static and Dynamic Electricity, 2nd. edition, McGraw-Hill Book Co. Inc., New York, p. 202, prob. 24C; 1950.

6) Bénéteau, P.J., L. Blaser and R.Q. Lane: Transistor Operational Amplifiers, Fairchild Technical Paper TP - 20/2, p. 3; Nov. 1962.

7) Heywood, D.R.: A Survey of Low-Noise Nucleonic Amplifiers, M.A.Sc. Thesis, University of British Columbia, pp. 14-27; Aug. 1963.

8) Blalock, T.V.: "A Low-Noise Charge-Sensitive Preamplifier with Field-Effect Transistor in the Input Stage", I.R.E. Trans. on Nucl. Sc., vol. NS-11, no. 4, pp. 365-372; June 1962.

9) Radeka, V.: "The Field-Effect Transistor - Its Characteristics and Applications", I.R.E. Trans. on Nucl. Sc., vol. NS-11, no. 4, pp. 358-364; June 1962.

10) Heywood, op. cit. 7, pp. 109-111.

11) Barnes, S.H. and G.G. Luettgenau: Design and Application of Insulated-Gate Field-Effect Transistors, T.R.W. Semiconductors Inc., p. 2; Nov. 1964.

12) Terman, F.E.: Electronic and Radio Engineering, 4th. edition, McGraw-Hill Book Co. Inc., New York, p. 298; 1955.

13) Rheinfelder, W.A.: *Design of Low-Noise Transistor Input Circuits*, Hayden Book Co. Inc., New York, p. 31; 1964.

14) Rothe, H. and W. Dahlke: "Theory of Noisy Fourpoles", *Proc. I.R.E.*, vol. 44, no. 6, pp. 811-818; June 1956.

15) Rheinfelder, op. cit. 13, p. 15.

16) Van der Ziel, A.: *Noise*, Prentice-Hall Inc., Englewood Cliffs, N.J., pp. 262-264; 1954.

17) Heiman, F.P. and S.R. Hofstein: "Metal-Oxide-Semiconductor Field-Effect Transistors", *Electronics*, vol. 37, no. 30, pp. 50-61; Nov. 30, 1964.

18) Jordan, A.G. and N.A. Jordan: "Theory of Noise in Metal Oxide Semiconductor Devices", *I.E.E.E. Trans. on Electron Devices*, vol. ED-12, no. 3, pp. 148-156; March 1965.

19) Van der Ziel, A.: "Gate Noise in Field-Effect Transistors at Moderately High Frequencies", *Proc. I.E.E.E.*, vol. 51, no. 3, pp. 461-467; March 1963.

20) Van der Ziel, A.: "Thermal Noise in Field-Effect Transistors", *Proc. I.R.E.*, vol. 50, no. 8, pp. 1808-1812; Aug. 1962.

21) Sevin, L.J.: *Field-Effect Transistors*, McGraw-Hill Book Co. Inc., New York, pp. 46-50; 1965.

22) Sevin, L.J. and S. Holcomb: "Field-Effect Transistors for Low-Level Circuits", chapt. 7, *Communications Handbook - Part I*, Miller, J.R. (ed.), Texas Instruments Microlibrary, Dallas, Texas, pp. 132-134; 1965.

23) Van der Ziel, op. cit. 20, p.1810.

24) Fairstein, E.: "Considerations in the Design of Pulse Amplifiers for use with Solid State Radiation Detectors", *I.R.E. Trans. on Nucl. Sc.*, vol. NS-8, no. 1, p. 129; Jan. 1961.

25) Blalock, op. cit. 8, p. 370.

26) Emmer, T.L.: "Low Noise Transistor Amplifiers for Solid State Detectors", *I.R.E. Trans. on Nucl. Sc.*, vol. NS-8, no. 1, pp. 140-146; Jan. 1961.

27) Hahn, J. and R. Mayer: " A Low Noise High Gain Bandwidth Charge Sensitive Preamplifier", *I.R.E. Trans. on Nucl. Sc.*, vol. NS-9, no. 3, pp 20-28; Aug. 1962.

28) Heywood, op. cit. 7, pp. 142-143.

29) Hahn and Mayer, op. cit. 27.

30) Warble, K.V. and N.J. Gri: "Integrated Circuit Charge-Sensitive Preamplifier", *I.E.E.E. Trans. on Nucl. Sc.*, vol. NS-13, no. 1, pp. 346-350; Feb. 1966.

31) Edwards, E.M.: *A D.C. Amplifier and Reference Voltage Supply Suitable for Use in a Magnetic Current Regulator*, M.Sc. Thesis, University of British Columbia, pp. 74-78; 1964.

32) Tombs, N.C. et al.: "A New Insulated-Gate Silicon Transistor", *Proc. I.E.E.E.*, Proc. Letters, vol. 54, no. 1, pp. 87-89; Jan. 1966.

33) Maguire, T.: "Silicon's New Wonder Drug", *Electronics*, vol. 39, no. 1, pp. 156-164; Jan. 10, 1966.

APPENDIX I

METAL-OXIDE-SEMICONDUCTOR FETS

The following description of the operation of a MOSFET is applicable to a P-channel enhancement type as shown in Figure A1.1. For an N-channel device all the voltage polarities are reversed. For a depletion type a drain current exists at zero gate voltage due to a native inversion layer.

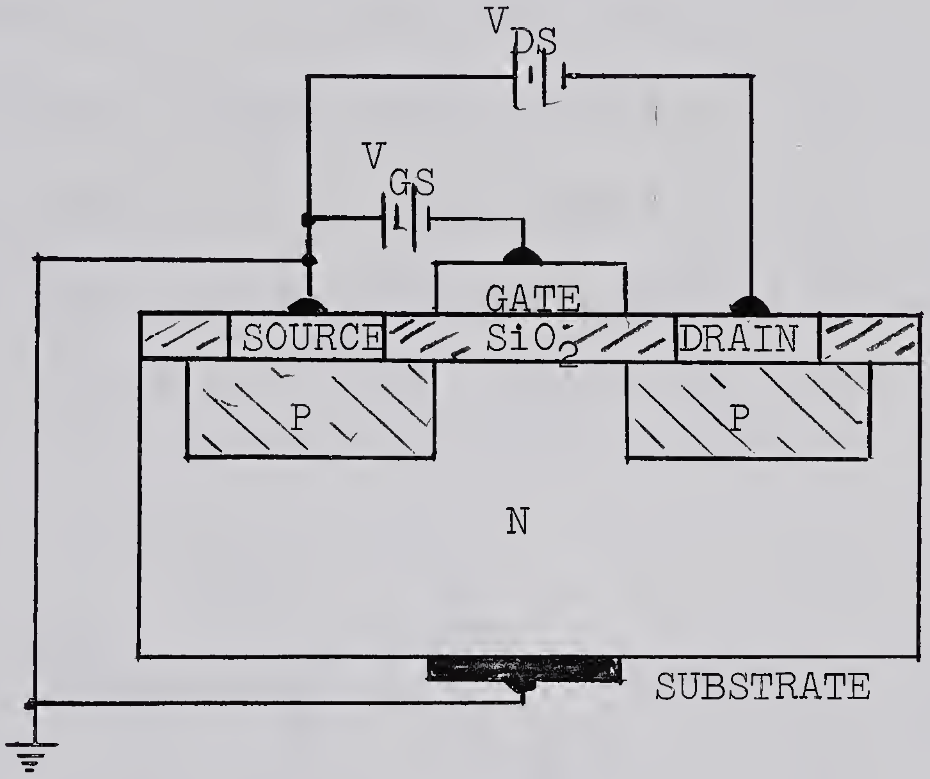

FIGURE A1.1 CROSS-SECTION OF A MOSFET

The source and drain are two P-islands diffused close together into an N-substrate and covered by an insulating layer of silicon dioxide. Metal electrodes are formed as shown. When the negative potential V_{GS} is applied, electrons in the N-channel are repelled from and holes are attracted to the insulating layer beneath the gate. Eventually, as

[illegible]

[illegible]

[illegible]

[illegible]

V_{GS} becomes more negative, the N-channel is converted into a P-channel, called the inversion layer, and drain current flows. The current flow is increased as V_{GS} is made more negative.

Initially this electronic conduction is essentially ohmic and takes place through the low resistance inversion layer. As the drain-to-source voltage, V_{DS}, is increased, the channel is pinched-off (as for a junction FET) and the drain current becomes almost constant. Pinch-off occurs when V_{DS} depletes the region around the drain of carriers.

The small-signal equivalent circuit for a 2N4120 is shown in Figure A1.2.* This is accurate to about 20 MHz.

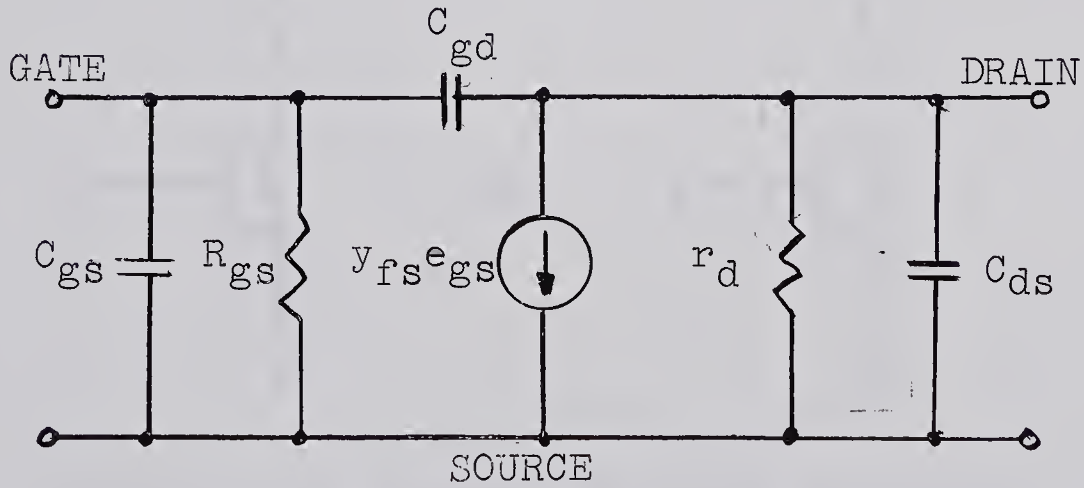

FIGURE A1.2 EQUIVALENT CIRCUIT OF A MOSFET

---

* MacDougall, J.S.: Applications of the Silicon Planar II MOS FET, Fairchild Application Bulletin APP-109; Nov. 1964.

APPENDIX II

REDUCTIONS TO EQUIVALENT TRANSISTORS

A2.1 Resistor-Transistor Combinations

The mixed h-parameters are given below for the equivalent transistors found from resistor-transistor combinations. Although some of the combinations were not used in the design of the charge-sensitive amplifier, all combinations are included for completeness. The exact equations are given. Simplifications are often possible but depend on the relative sizes of the resistances and parameters involved. Of course, any impedance can be used in place of the resistors.

A2.1.1 Emitter Resistor

This case is shown in Figure A2.1a.

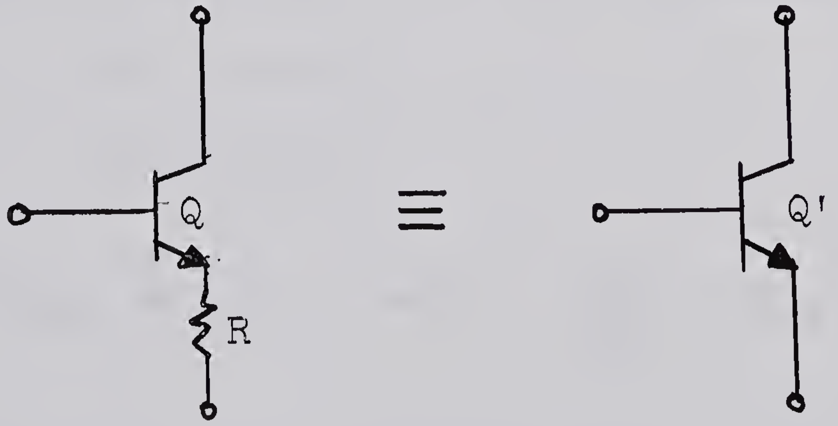

FIGURE A2.1a EMITTER RESISTOR REDUCTION

The common base h-parameter model, including R, is shown in Figure A2.1b.

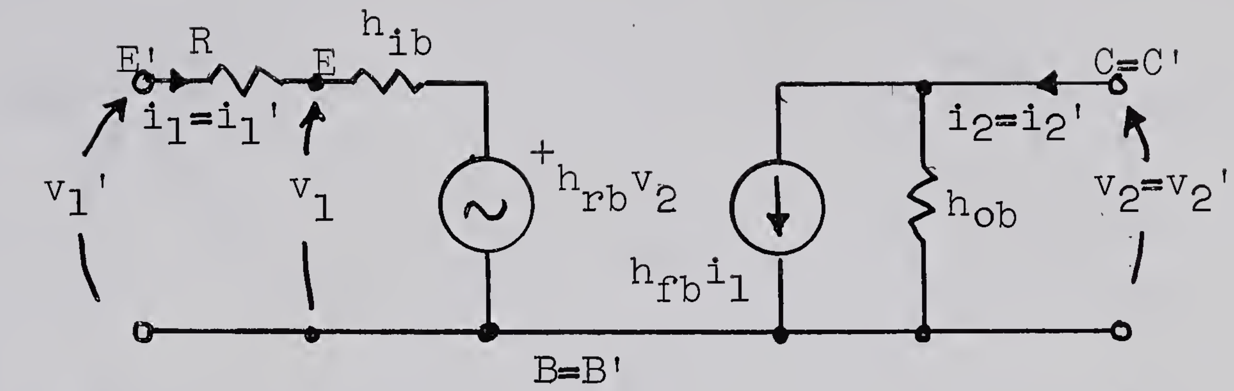

FIGURE A2.1b COMMON BASE MODEL

The defining equations are:

$$v_1 = h_{ib}i_1 + h_{rb}v_2 \qquad v_1' = h_{ib}'i_1' + h_{rb}'v_2'$$

$$i_2 = h_{fb}i_1 + h_{ob}v_2 \qquad i_2' = h_{fb}'i_1' + h_{ob}'v_2'$$

To solve for h_{rb}' and h_{ob}', let $i_1' = 0$ and apply v_2'.

Then:

$$v_1' = h_{rb}v_2'$$

$$i_2' = h_{ob}v_2'$$

$$\frac{v_1'}{v_2'} = h_{rb}' = h_{rb} \quad \text{and} \quad \frac{i_2'}{v_2'} = h_{ob}' = h_{ob}$$

To solve for h_{ib}', let $v_2' = 0$ and apply i_1'.

Then:

$$v_1' = i_1'(h_{ib} + R)$$

$$\frac{v_1'}{i_1'} = h_{ib}' = h_{ib} + R$$

To find h_{fe}' it is easiest to use the common emitter model and then substitute the mixed h-parameters for the common

emitter parameters. The common emitter model is shown in Figure A2.1c.

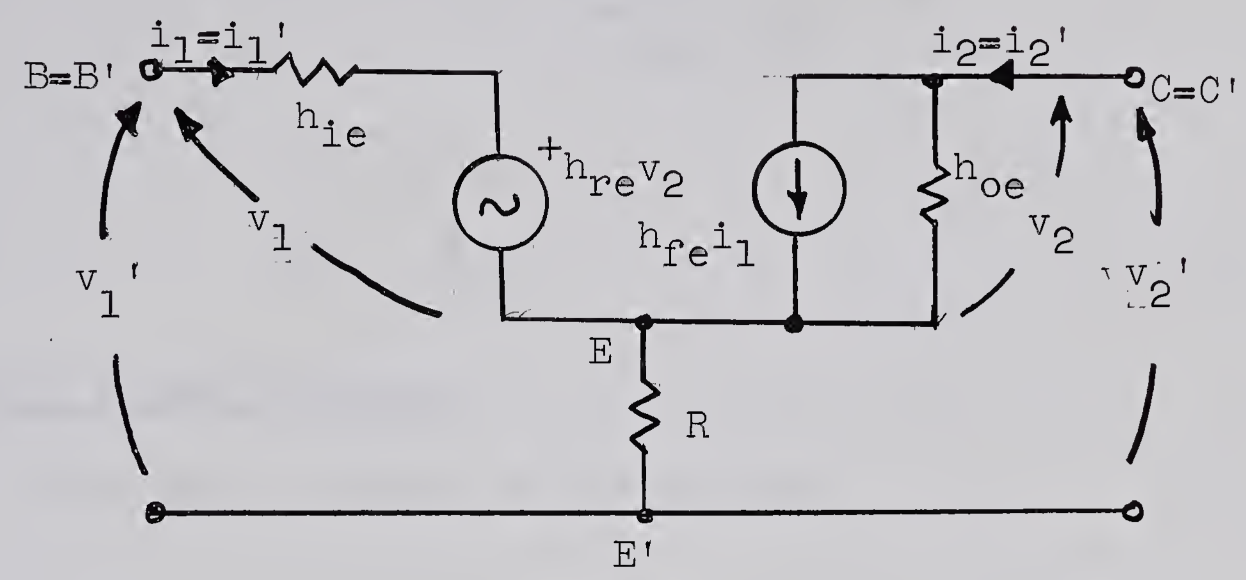

FIGURE A2.1c COMMON EMITTER MODEL

To determine h_{fe}', let $v_2' = 0$ and apply i_1'.

Then:

$$i_2' = h_{fe}i_1' + h_{oe}v_2$$

$$v_2 = -(i_1' + i_2')R$$

$$\frac{i_2'}{i_1'} = h_{fe}' = \frac{h_{fe} - h_{oe}R}{1 + h_{oe}R}$$

Substituting $h_{oe} = \frac{1+h_{fe}}{1-h_{rb}} h_{ob}$ yields:

$$h_{fe}' = \frac{h_{fe} - \frac{1+h_{fe}}{1-h_{rb}} h_{ob}R}{1 + \frac{1+h_{fe}}{1-h_{rb}} h_{ob}R}$$

Therefore the exact equations are:

$$h_{ib}' = h_{ib} + R$$

$$h_{fe}' = \frac{h_{fe} - \frac{1+h_{fe}}{1-h_{rb}} h_{ob}R}{1 + \frac{1+h_{fe}}{1-h_{rb}} h_{ob}R}$$

$$h_{rb}' = h_{rb}$$

$$h_{ob}' = h_{ob} \qquad (A2.1)$$

A2.1.2 Base Resistor

This case is shown in Figure A2.2.

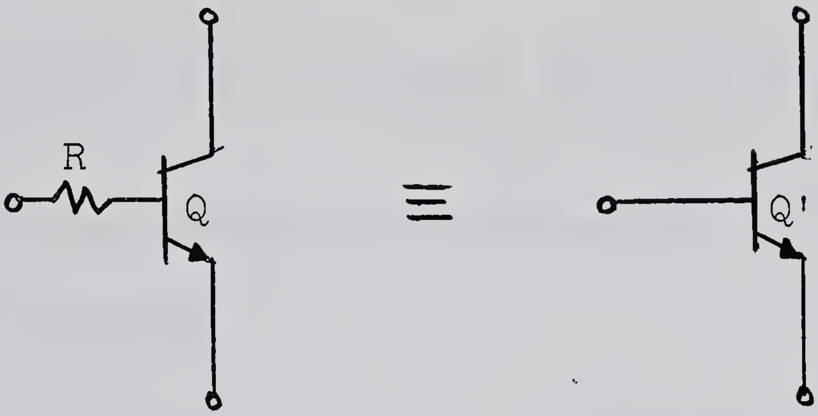

FIGURE A2.2 BASE RESISTOR REDUCTION

From an analysis similar to that used in A2.1.1, the exact equations are:

$$h_{ib}' = h_{ib} + \frac{R}{1+h_{ob}R}\,\frac{1}{1+h_{fe}}\left[1 - (1+h_{fe})h_{ib}h_{ob}\right]$$

$$h_{fe}' = h_{fe}$$

$$h_{rb}' = \frac{h_{rb} + h_{ob}R}{1 + h_{ob}R}$$

$$h_{ob}' = \frac{h_{ob}}{1 + h_{ob}R} \qquad (A2.2)$$

A2.1.2 Collector Resistor

This case is shown in Figure A2.3.

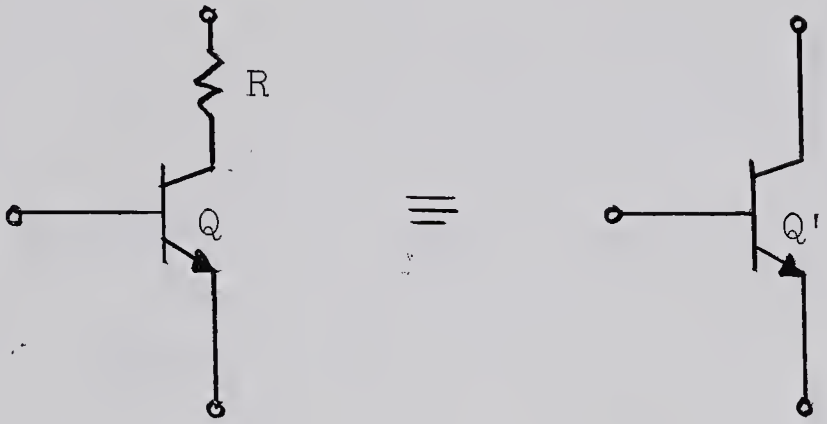

FIGURE A2.3 COLLECTOR RESISTOR REDUCTION

From an analysis similar to that used in A2.1.1, the exact equations are:

$$h_{ib}' = h_{ib} + \frac{\dfrac{h_{fe}}{1+h_{fe}} + \dfrac{h_{ib}h_{ob}}{1-h_{rb}}}{1 + h_{ob}R} h_{rb}R$$

$$h_{fe}' = \frac{h_{fe}}{1 + \dfrac{1+h_{fe}}{1-h_{rb}} h_{ob}R}$$

$$h_{rb}' = \frac{h_{rb}}{1 + h_{ob}R}$$

$$h_{ob}' = \frac{h_{ob}}{1 + h_{ob}R} \qquad (A2.3)$$

A2.1.4 Base-Emitter Resistor

This case is shown in Figure A2.4.

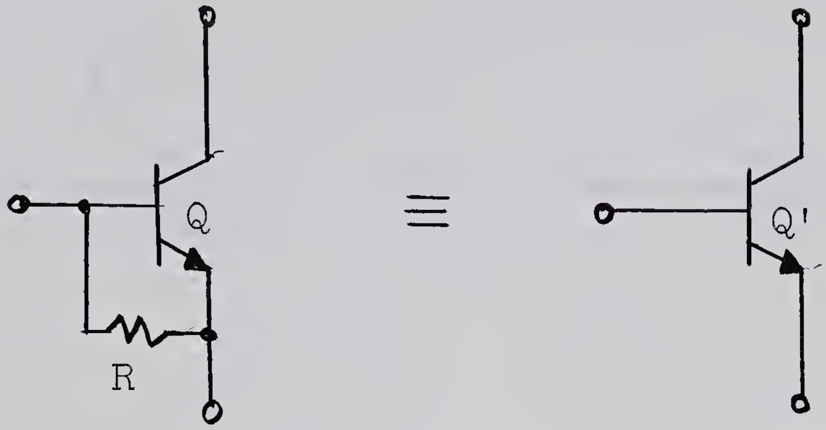

FIGURE A2.4 BASE-EMITTER RESISTOR REDUCTION

From an analysis similar to that used in A2.1.1, the exact equations are:

$$h_{ib}' = \frac{h_{ib}}{1 + \frac{h_{ib}}{R}}$$

$$h_{fe}' = \frac{h_{fe}}{1 + \frac{h_{ib}(1+h_{fe})}{R(1-h_{rb})}}$$

$$h_{rb}' = \frac{h_{rb}}{1 + \frac{h_{ib}}{R}}$$

$$h_{ob}' = h_{ob} + \frac{\frac{h_{fe}}{1+h_{fe}} h_{rb}}{h_{ib} + R} \left[1 + \frac{1+h_{fe}}{h_{fe}} \frac{h_{ob}h_{ib}}{1-h_{rb}} \right] \qquad (A2.4)$$

A2.1.5 Collector-Base Resistor

This case is shown in Figure A2.5.

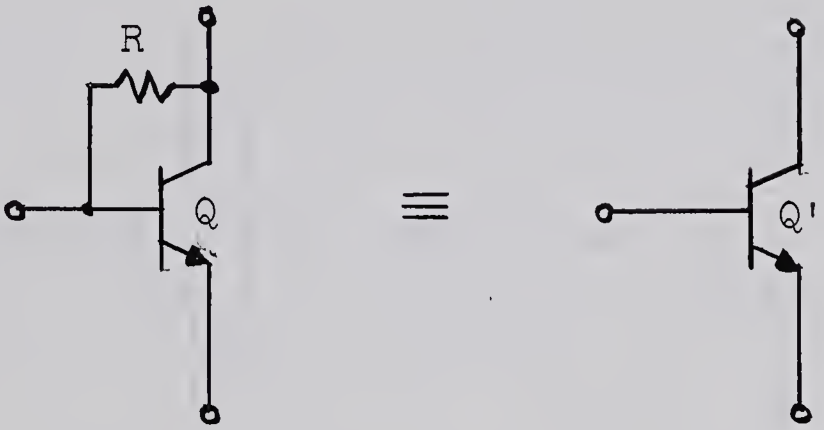

FIGURE A2.5 COLLECTOR-BASE RESISTOR

From an analysis similar to that used in A2.1.1, the exact equations are:

$$h_{ib}' = h_{ib}$$

$$h_{fe}' = h_{fe} \frac{R - \frac{1+h_{fe}}{h_{fe}} \frac{h_{ib}}{1-h_{rb}}}{R + \frac{1+h_{fe}}{1-h_{rb}} h_{ib}}$$

$$h_{rb}' = h_{rb}$$

$$h_{ob}' = \frac{1 + h_{ob}R}{R} \qquad (A2.5)$$

A2.1.6 Collector-Emitter Resistor

This case is shown in Figure A2.6.

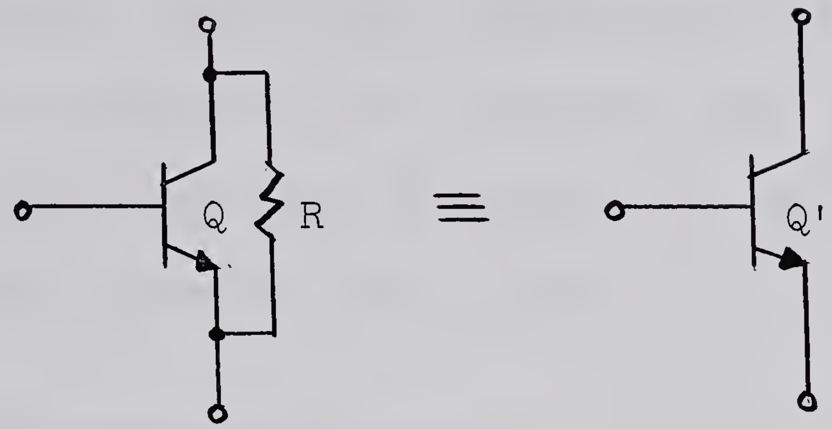

FIGURE A2.6 COLLECTOR-EMITTER RESISTOR REDUCTION

From an analysis similar to that used in A2.1.1, the exact equations are:

$$h_{ib}' = \frac{h_{ib}R}{h_{ib} + R}$$

$$h_{fe}' = h_{fe}$$

$$h_{rb}' = h_{rb} + \frac{h_{ib}}{h_{ib} + R}(1 - h_{rb})$$

$$h_{ob}' = h_{ob} + \frac{\frac{1-h_{rb}}{1+h_{fe}} - h_{ob}h_{ib}}{h_{ib} + R} \qquad \text{(A2.6)}$$

[illegible]

[illegible]

[illegible]

[illegible]

[illegible]

[illegible]

[illegible]

[illegible]

[illegible]

A2.2 Transistor-Transistor Combinations

Two transistor-transistor compounds were used in the charge-sensitive amplifier. The complementary compound used in the output emitter follower has been analyzed by Edwards* and the "almost" exact mixed h-parameters are given below. For the FET-transistor hybrid compound used in the input stage the exact admittance parameters, as well as appropriate "almost" exact equations, are given.

A2.2.1 Complementary Compound

The compound is equivalent to a single transistor as shown in Figure A2.7.

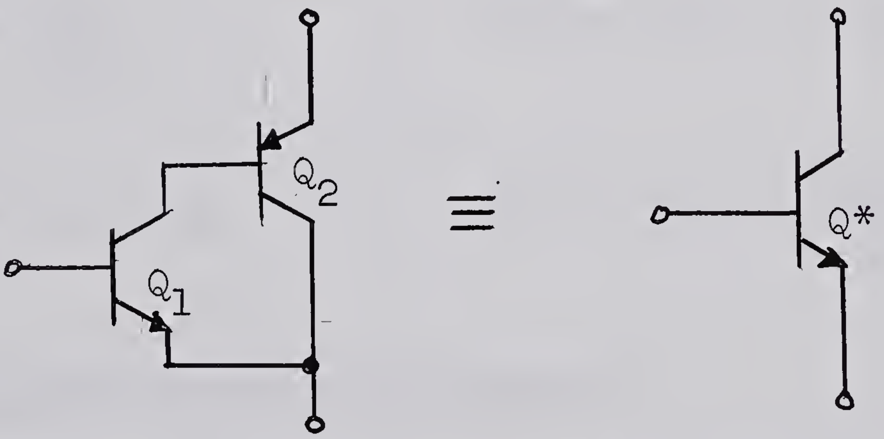

FIGURE A2.7 COMPLEMENTARY COMPOUND

---

* Edwards, E.M.: A D.C. Amplifier and Reference Voltage Supply Suitable for Use in a Magnetic Current Regulator, M.Sc. Thesis, University of British Columbia, pp. 74-78; 1964.

The mixed h-parameters (assuming $h_{fe} \gg 1$ and $h_{rb} \ll 1$)are:

$$h_{ib}^* = \frac{h_{ib1}}{h_{fe2}} + h_{ib2}(h_{ob1}h_{ib1} + h_{rb1})$$

$$h_{fe}^* = \frac{h_{fe1}h_{fe2}}{1 + h_{fe1}h_{fe2}h_{ob1}h_{ib2}}$$

$$h_{rb}^* = h_{rb1} + h_{ib1}h_{ob2} + h_{fe}^*h_{ib1}h_{ib2}(h_{ob1})^2$$

$$h_{ob}^* = h_{ob1} + \frac{h_{ob2}}{h_{fe1}} \qquad \text{(A2.7a)}$$

Generally the following approximate equations apply:

$$h_{ib}^* \simeq \frac{h_{ib1}}{h_{fe2}} \qquad h_{rb}^* \simeq h_{rb1} + h_{ib1}h_{ob2}$$

$$h_{fe}^* \simeq h_{fe1}h_{fe2} \qquad h_{ob}^* = h_{ob1} + \frac{h_{ob2}}{h_{fe1}} \qquad \text{(A2.7b)}$$

A2.2.2 MOSFET-Transistor Compound

The compound is equivalent to a single MOSFET as shown in Figure A2.8. For a MOSFET the input admittance, y_{is}, and the reverse feedback admittance, y_{rs}, can normally be neglected at the frequencies encountered in the use of the charge-sensitive amplifier.

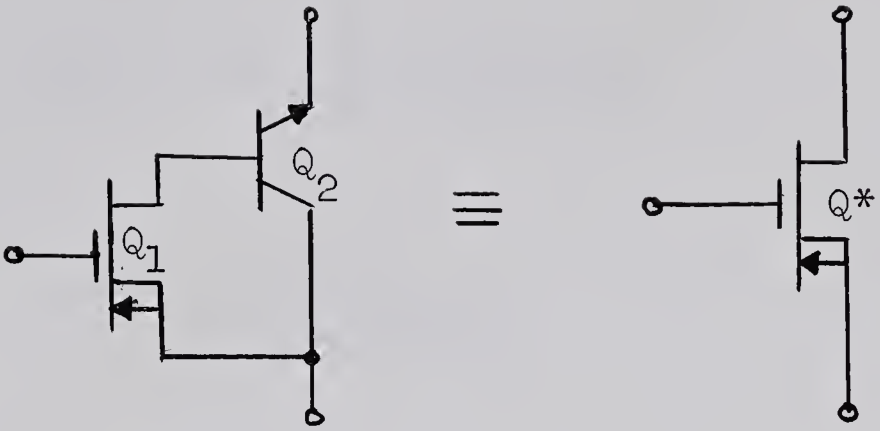

FIGURE A2.8 MOSFET-TRANSISTOR COMPOUND

Using the y-parameter model for the MOSFET and the h-parameter model for the junction transistor, with the appropriate interconnections, the exact equations (the mixed h-parameters are used for the junction transistor) are found to be:

$$y_{is}^* = y_{is} - \frac{y_{rs} y_{fs}(1+h_{fe})}{(1-h_{rb})} \frac{h_{ib}}{1 + h_{ib} y_{os} \dfrac{(1+h_{fe})}{(1-h_{rb})}}$$

$$y_{fs}^* = \frac{y_{fs}(1+h_{fe})}{1 + h_{ib} y_{os} \dfrac{(1+h_{fe})}{(1-h_{rb})}}$$

$$y_{rs}^* = \frac{y_{rs}}{1-h_{rb}} \frac{1 - h_{ib} h_{ob} \dfrac{(1+h_{fe})}{(1-h_{rb})}}{1 + h_{ib} y_{os} \dfrac{(1+h_{fe})}{(1-h_{rb})}}$$

$$y_{os}^* = (y_{os} + h_{ob}) \frac{1+h_{fe}}{1-h_{rb}} \frac{1}{1 + h_{ib} y_{os} \dfrac{(1+h_{fe})}{(1-h_{rb})}} \qquad \text{(A2.8a)}$$

For $h_{fe} \gg 1$ and $h_{rb} \ll 1$:

$$y_{is}^* \simeq y_{is} - \frac{y_{rs} y_{fs} h_{fe} h_{ib}}{1 + y_{os} h_{fe} h_{ib}}$$

$$y_{fs}^* \simeq \frac{h_{fe} y_{fs}}{1 + y_{os} h_{fe} h_{ib}}$$

$$y_{rs}^* \simeq y_{rs} \frac{1 - h_{ob} h_{fe} h_{ib}}{1 + y_{os} h_{fe} h_{ib}}$$

$$y_{os}^* \simeq \frac{h_{fe}(y_{os} + h_{ob})}{1 + y_{os} h_{fe} h_{ib}} \qquad \text{(A2.8b)}$$

APPENDIX III

EXPERIMENTAL EXCESS NOISE IN MOSFETS

Preliminary measurements of the noise performance of the charge-sensitive amplifier indicated that the 1/f noise of MOSFETs is much more predominant than was originally thought. Therefore it was decided to measure the noise, to confirm that it was 1/f in character, and to determine the 1/f noise-power corner frequency.

Two similar methods of measurement were used to determine the value of the 1/f noise-power corner frequency. The basic system used for both methods was the same and is shown in Figure A3.1.

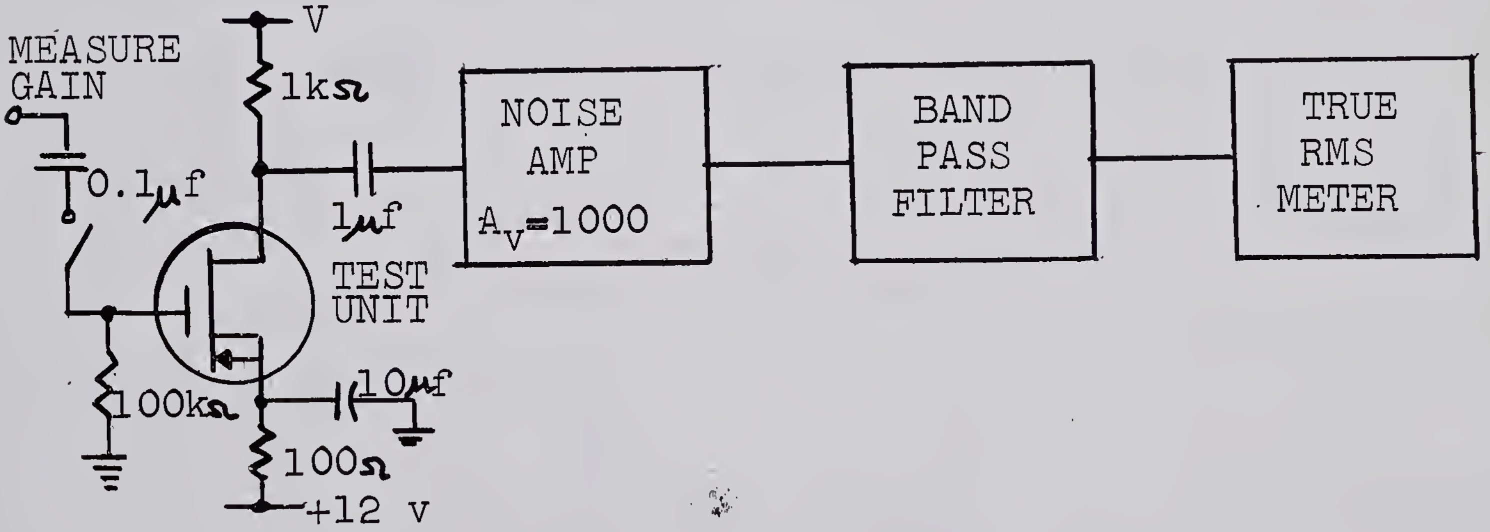

FIGURE A3.1 NOISE MEASUREMENT SYSTEM

The device under test was set to the operating conditions of the MOSFET in the charge-sensitive amplifier, V_{GS} = -12 volts and V_{DS} = -7 volts. The quiescent current and the

transconductance of each device were measured under these conditions. The output noise was measured with the test unit in place (e_2) and also with a resistor equal to the test unit output impedance substituted for the test unit (e_1). Also, the system gain was measured with the test unit in place. Both noise voltages were referred to the system input (the input voltages are denoted by $\overline{n_2}$ and $\overline{n_1}$). The equivalent input noise of the test device is then, $\overline{n^2} = \overline{n_2}^2 - \overline{n_1}^2$.

In the first method three 2N4120's and a General Microelectronics' 2N3610 were tested. A KhronHite band-pass filter was used. This filter has -80 db/dec roll-offs, but for simplicity the roll-offs were assumed to be infinite. This results in an error of about 13% *

For leakage (since the source is resistive) and thermal noise:

$$\overline{n_t}^2 \propto \int_{f_L}^{f_H} df = f_H - f_L \tag{A3.1}$$

And for 1/f noise:

$$\overline{n_f}^2 \propto \int_{f_L}^{f_H} \frac{1}{f}\, df = \ln \frac{f_H}{f_L} \tag{A3.2}$$

When the ratio of f_H/f_L was kept constant the noise remained the same, indicating that the noise is 1/f in character.

* Rheinfelder, W.A.: Design of Low-Noise Transistor Input Circuits, Hayden Book Co. Inc., New York, p. 17; 1964.

As a check on the first method, simple and equal differentiating and integrating time constant filters were used as the band-pass filter. This filter is shown in Figure A3.2. Then the gain expression is:

$$\left| A(\omega) \right|^2 = \frac{\omega_c^2 A_o^2 \omega^2}{(\omega_c^2 + \omega^2)^2} \qquad \text{(A3.3)}$$

where: ω_c is the cutoff frequency.

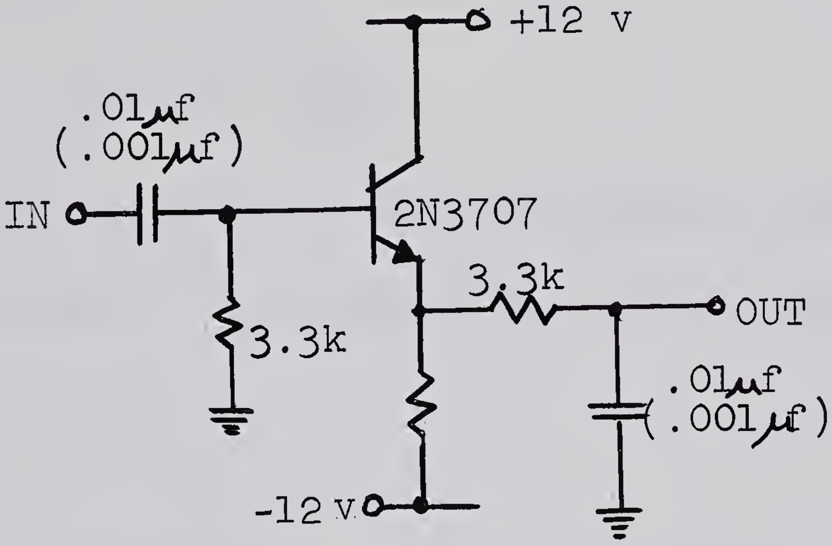

FIGURE A3.2 BAND-PASS FILTER

For thermal and leakage noise:

$$\bar{n}_t^2 \propto \omega_c^2 \int_0^{\infty} \frac{\omega^2}{(\omega_c^2 + \omega^2)^2} \, d\omega = \frac{1}{4}\omega_c \qquad \text{(A3.4)}$$

And for 1/f noise:

$$\bar{n}_t^2 \propto \omega_c^2 \int_0^{\infty} \frac{\omega}{(\omega_c^2 + \omega^2)^2} \, d\omega = \frac{1}{2} \qquad \text{(A3.5)}$$

The noise was measured for two different time constants and remained the same. This again indicates that the noise is 1/f in character. This method was used for only one transistor, a 2N4120.

The noise-power corner frequency for method 1 can be calculated from:

$$f_{CF} = \frac{\overline{n^2}}{\ln f_H/f_L} \frac{y_{fs}}{4kT} \qquad \text{(A3.6)}$$

And for method 2:

$$f_{CF} = 2\overline{n^2} \frac{y_{fs}}{4kT} \qquad \text{(A3.7)}$$

The noise was measured using a Hewlett-Packard 3400 true rms voltmeter. The noise-power corner frequencies are:

Method 1

2N4120 #1 $f_{CF} = 30.7$ MHz

2N4120 #2 $f_{CF} = 15.6$ MHz

2N4120 #3 $f_{CF} = 34.4$ MHz

2N3610 $f_{CF} = 29.4$ MHz

Method 2

2N4120 #1 $f_{CF} = 28.5$ MHz

The frequencies obtained from method 1 were corrected to account for the finite roll-offs of the band-pass filter.

To determine the effect of the operating point on the 1/f noise a 2N4120 was operated at various drain currents between 100 μa and 10 ma and various drain-to-source voltages between -4 volts and -16 volts. No substantial change in the input noise voltage was noticed. In fact, over these ranges the maximum change was 5%. However, changes in the operating conditions can have a profound effect on the thermal noise contribution.